Department of Applied Physics

Novel approaches to the analysis of nuclear and other radioactive materials

Improving detection capability through alpha-gamma coincidence, alpha-induced optical fluorescence and advanced spectrum analysis

Sakari Ihantola

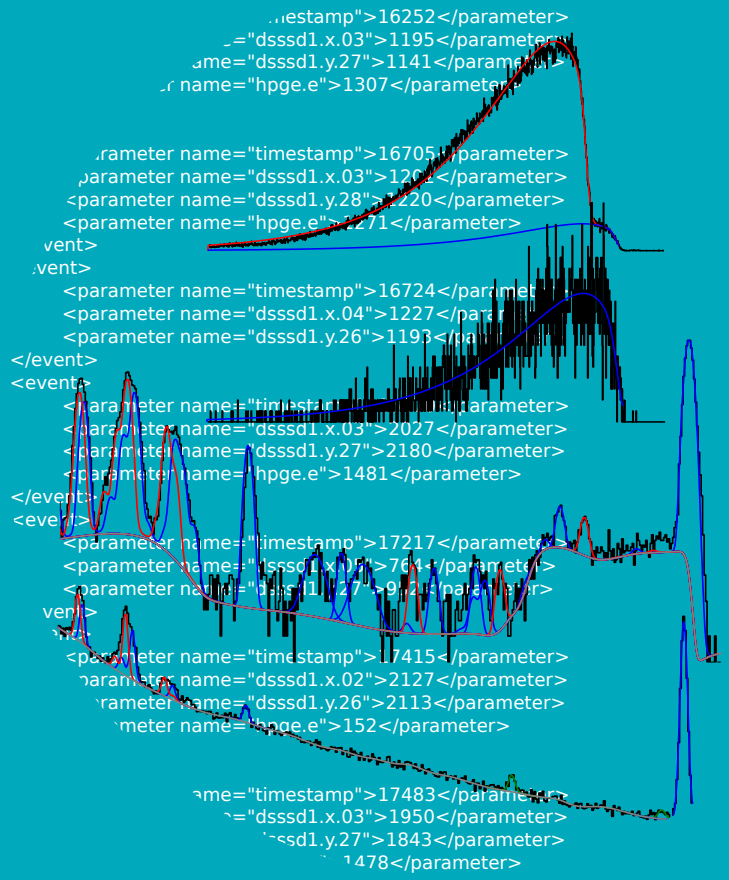

Aalto University

DOCTORAL DISSERTATIONS

Aalto University publication series
DOCTORAL DISSERTATIONS 198/2013

Novel approaches to the analysis of nuclear and other radioactive materials

Improving detection capability through alpha-gamma coincidence, alpha-induced optical fluorescence and advanced spectrum analysis

Sakari Ihantola

A doctoral dissertation completed for the degree of Doctor of Science (Technology) to be defended, with the permission of the Aalto University School of Science, at a public examination held at the lecture hall F239a of the school on 13 December 2013 at 12.

Aalto University
School of Science
Department of Applied Physics
Fission and Radiation Physics

Supervising professor
Prof. Rainer Salomaa

Thesis advisor
Dr Harri Toivonen, STUK - Radiation and Nuclear Safety Authority, Finland

Preliminary examiners
Prof. Paul Greenlees, University of Jyväskylä, Finland

Dr Georgi Pavlovski, Symetrica Security Ltd, United Kingdom

Opponent
Prof. Steven Biegalski, The University of Texas at Austin, United States of America

Aalto University publication series
DOCTORAL DISSERTATIONS 198/2013

ISBN 978-952-60-5460-5
ISBN 978-952-60-5461-2 (pdf)
ISSN-L 1799-4934
ISSN 1799-4934 (printed)
ISSN 1799-4942 (pdf)
http://urn.fi/URN:ISBN:978-952-60-5461-2

Unigrafia Oy
Helsinki 2013

Finland

441 697
Printed matter

Aalto University

Abstract

Aalto University, P.O. Box 11000, FI-00076 Aalto www.aalto.fi

Author
Sakari Ihantola

Name of the doctoral dissertation
Novel approaches to the analysis of nuclear and other radioactive materials

Publisher School of Science

Unit Department of Applied Physics

Series Aalto University publication series DOCTORAL DISSERTATIONS 198/2013

Field of research Advanced Energy Systems

Manuscript submitted 9 September 2013 **Date of the defence** 13 December 2013

Permission to publish granted (date) 7 November 2013 **Language** English

☐ **Monograph** ☒ **Article dissertation (summary + original articles)**

Abstract

Nuclear and other radioactive materials pose a special concern in the proliferation of nuclear weapons, reactor accidents or through criminal acts. To prevent the adverse effects of the use of these materials, novel approaches for their detection and analysis are required. The objective of the research in this thesis was to improve the detection and characterisation of nuclear and other radioactive materials with radiometric methods.

Radioactive sources can be detected and identified based on their radiation, such as alpha particles or gamma rays, emitted in the decay of unstable atoms. In practice, background radiation and attenuation impair the minimum detectable activity. In this thesis, the simultaneous detection of both gamma rays and alpha particles originating from the same decay was shown to increase the detection sensitivity of certain radionuclides compared to the equivalent separate measurements. Unfortunately, the measurement geometry in this direct alpha-gamma coincidence approach can be limited by the short range of alpha particles in air. This deficiency was overcome for the first time by the use of coincidences between gamma rays and secondary optical photons. The secondary optical photons are produced during the flight of alpha particles in air.

In addition to the measurement techniques, statistical uncertainties were investigated both in spectrum fitting and in the interpretation of the results. The techniques were applied to the analysis of gamma-ray and alpha-particle spectra. Emphasis was placed on the correlated variables and analysis of data with limited statistics.

The techniques presented improve the analysis of radioactive materials in several applications. The alpha-gamma coincidence technique is especially suited to the analysis of plutonium samples, which is important for nuclear safeguards. Nuclear decommissioning and crime scene investigation would greatly benefit from the capability to detect alpha-particle emitters at a stand-off distance. The reliability of the analysis algorithms is particularly crucial in portal monitors and other applications where weak signals from a large number of spectra are automatically inquired without expert support.

Keywords gamma-ray spectrometry, alpha-particle spectrometry, covariance analysis, coincidence measurement, remote alpha-particle detection, UV-fluorescence

ISBN (printed) 978-952-60-5460-5 **ISBN (pdf)** 978-952-60-5461-2

ISSN-L 1799-4934 **ISSN (printed)** 1799-4934 **ISSN (pdf)** 1799-4942

Location of publisher Helsinki **Location of printing** Helsinki **Year** 2013

Pages 141 **urn** http://urn.fi/URN:ISBN:978-952-60-5461-2

Aalto-yliopisto

Tiivistelmä

Aalto-yliopisto, PL 11000, 00076 Aalto www.aalto.fi

Tekijä
Sakari Ihantola

Väitöskirjan nimi
Uudenlainen lähestymistapa ydinmateriaalien ja muiden radioaktiivisten aineiden analyysiin

Julkaisija Perustieteiden korkeakoulu

Yksikkö Teknillisen fysiikan laitos

Sarja Aalto University publication series DOCTORAL DISSERTATIONS 198/2013

Tutkimusala Energiatieteet

Käsikirjoituksen pvm 09.09.2013 **Väitöspäivä** 13.12.2013

Julkaisuluvan myöntämispäivä 07.11.2013 **Kieli** Englanti

☐ **Monografia** ☒ **Yhdistelmäväitöskirja (yhteenveto-osa + erillisartikkelit)**

Tiivistelmä

Radioaktiivisten aineiden ja ydinmateriaalien käyttö vaatii viranomaisvalvontaa. Radioaktiivisten aineiden lähettämä säteily aiheuttaa vakavan uhan sekä onnettomuustilanteissa että lähteiden joutuessa rikollisten käsiin. Ydinmateriaaleja voidaan lisäksi käyttää ydinaseiden valmistukseen. Jotta näitä materiaaleja voitaisiin hyödyntää turvallisesti ja estää niiden lainvastainen käyttö, tarvitaan tehokkaita havaitsemis- ja tunnistamismenetelmiä. Tässä väitöskirjassa keskitytään radiometrisiin analyysimenetelmiin.

Säteilylähteen tunnistus perustuu radioaktiivisissa hajoamisissa syntyvään säteilyyn, kuten alfahiukkasiin tai suurienergisiin fotoneihin. Menetelmien haasteena on erottaa tutkittavan kohteen lähettämä säteily muista lähteistä johtuvasta taustasäteilystä. Tässä työssä osoitetaan tunnistamisen helpottuvan, kun hyödynnetään samassa radioaktiivissa hajoamisessa syntyneiden alfahiukkasten ja fotonien yhtäaikaista havaitsemista. Menetelmän käyttöä kuitenkin rajoittaa alfahiukkasten vain muutaman senttimetrin kantama ilmassa. Tämä ongelma ratkaistaan työssä ensimmäistä kertaa mittaamalla yhtä aikaa gammafotoneja ja optisia fotoneja, jotka syntyvät alfahiukkasten virittäessä ilman typpimolekyylejä.

Mittaustekniikoiden kehittämisen lisäksi työssä tutkitaan tilastollisia epävarmuuksia spektrianalyysissä ja tulosten tulkinnassa. Menetelmiä sovelletaan sekä alfa- että gammaspektrien analyysiin. Erityisesti kiinnitetään huomiota korreloituneiden suureiden virhearviointiin ja vähäisiä pulssimääriä sisältävän datan käsittelyyn.

Esitetyillä tekniikoilla on monia sovelluskohteita radioaktiivisten aineiden analyysissä. Alfahiukkasten ja gammasäteilyn samanaikainen mittaus soveltuu erityisesti ydinasevalvonnan kannalta keskeisten plutoniumisotooppien analyysiin. Alfahiukkasten ilmassa tuottamien optisten fotonien mahdollistamaa etähavainnointia voidaan hyödyntää muun muassa pinnoille tarttuneen radioaktiivisen saasteen havainnoinnissa ja tunnistamisessa. Tällainen pintakontaminaatio voi aiheuttaa vakavan terveysriskin esimerkiksi ydinlaitoksia purettaessa. Analyysialgoritmin luotettavuuden merkitys korostuu sovelluksissa, joissa säteilyä mitataan automaattisesti ilman säteilyasiantuntijaa.

Avainsanat gammaspektrometria, alfaspektrometria, kovarianssianalyysi, koinsidenssimittaus, alfasäteilyn etähavainnointi, UV-fluoresenssi

ISBN (painettu) 978-952-60-5460-5 **ISBN (pdf)** 978-952-60-5461-2

ISSN-L 1799-4934 **ISSN (painettu)** 1799-4934 **ISSN (pdf)** 1799-4942

Julkaisupaikka Helsinki **Painopaikka** Helsinki **Vuosi** 2013

Sivumäärä 141 **urn** http://urn.fi/URN:ISBN:978-952-60-5461-2

Preface

The work presented in this thesis was carried out in the Finnish Radiation and Nuclear Safety Authority, STUK. The majority of the study was accomplished in the laboratory for Security Technology during the years 2009-2013.

My foremost gratitude goes to my advisor, Dr Harri Toivonen, and supervisor, Prof. Rainer Salomaa. The innovative ideas of Dr Toivonen and his infectious enthusiasm have helped me to overcome the challenges arisen during this thesis work. I am thankful for both the insightful guidance of Prof. Salomaa upon preparing this thesis, as well as for his long-term advisement in radiation and nuclear physics since 2005.

I could not have received better pre-examiners than Prof. Paul Greenlees and Dr Georgi Pavlovski. Multiple aspects of this thesis were enhanced based on their comments. Prof. Greenlees gave worthy ideas for further studies and pointed out the importance of precise, scientific expressions. I was impressed by the level of mathematical analysis that Dr Pavlovski showed on the presented statistic theory.

I am grateful for the possibility to participate in so many interesting research projects with brilliant and agile people. The knowledge of Dr Kari Peräjärvi on novel measurement approaches has been the driving force for the innovative measurement techniques presented. My special thanks also go to my other co-authors: Mr Mikael Moring, Mr Andreas Pelikan, Dr Roy Pöllänen, Mr Johan Sand, Dr Juha Toivonen and Dr Jani Turunen. Their contribution to the publications included in this thesis has been irreplaceable and I could not have been able to accomplish this work without them. I have been lucky to have such good colleagues as Mr Philip Holm, Ms Tarja Ilander, Mr Tero Karhunen, Mr Samu Ristikari, Mr Ari-Pekka Sihvonen, Mr Petri Smolander and Ms Nina Sulonen, to

mention just a few. I am very grateful for the time they have always found to help me regardless of the often tight schedules.

My final thanks go to my family and friends. The time spent together has provided me with valuable breaks from writing this thesis. My parents have supported me throughout my studies as well as encouraged me to learn and explore new things. My wife, Laura, has brought light and grammar to my life.

Helsinki, November 30, 2013,

Sakari Ihantola

Contents

Preface **vii**

Contents **ix**

List of Publications **xi**

Author's Contribution **xiii**

1. Introduction **1**

1.1 Characterisation of nuclear material 2

1.2 Objectives of the work 4

2. Statistical methods **7**

2.1 Limit of detectability 7

2.2 Fitting 13

2.3 Combined uncertainty of dependent variables 15

2.4 Conclusions 17

3. Analysis of gamma-ray spectra **19**

3.1 AMUFI analysis software 20

3.2 Statistical properties 23

3.3 Application to dating of a nuclear release 24

3.4 Conclusions 27

4. Analysis of alpha-particle spectra **29**

4.1 ADAM analysis software 30

4.2 Statistical properties 34

4.3 Application to plutonium analysis 36

4.4 Conclusions 38

5. Alpha-gamma coincidence **39**

5.1 Methods for activity determination 40
5.2 PANDA testbed for coincidence studies 42
5.3 Application to characterisation of a nuclear bomb particle . 43
5.4 Conclusions 46

6. UV-gamma coincidence **49**
6.1 Alpha-induced UV fluorescence 49
6.2 Capabilities of UV-gamma coincidence 52
6.3 Conclusions 55

7. Discussion and conclusions **57**
7.1 Implications 58
7.2 Limits of the techniques 60
7.3 Future research 61

List of Publications

This thesis consists of an overview and of the following publications which are referred to in the text by their Roman numerals.

I K. Peräjärvi, S. Ihantola, R. Pöllänen, H. Toivonen, J. Turunen. Determination of ^{235}U, ^{239}Pu, ^{240}Pu, and ^{241}Am in a Nuclear Bomb Particle Using a Position-Sensitive α-γ Coincidence Technique. *Environmental Science & Technology*, 45, 4, 1528-1533, January 2011.

II S. Ihantola, A. Pelikan, R. Pöllänen, H. Toivonen. Advanced Alpha Spectrum Analysis Based on the Fitting and Covariance Analysis of Dependent Variables. *Nuclear Instruments and Methods in Physics Research A*, 656, 11, 55-60, November 2011.

III R. Pöllänen, T. Siiskonen, S. Ihantola, H. Toivonen, A. Pelikan, K. Inn, J. La Rosa, B.J. Bene. Determination of ^{239}Pu/^{240}Pu Isotopic Ratio by High-Resolution Alpha-Particle Spectrometry Using the ADAM Program. *Applied Radiation and Isotopes*, 70, 4, 733-739, April 2012.

IV S. Ihantola, J. Sand, K. Peräjärvi, J. Toivonen, H. Toivonen. Principles of UV–Gamma Coincidence Spectrometry. *Nuclear Instruments and Methods in Physics Research A*, 690, 21, 79-84, October 2012.

V S. Ihantola, J. Sand, K. Peräjärvi, J. Toivonen, H. Toivonen. Fluorescence-Assisted Gamma Spectrometry for Surface Contamination Analysis. *IEEE Transactions on Nuclear Science*, 60, 1, 305-309, February 2013.

VI S. Ihantola, H. Toivonen, M. Moring. ^{140}La/^{140}Ba Ratio Dating of a Nuclear Release. *Journal of Radioanalytical and Nuclear Chemistry*, 298, 2, 1283-1291, November 2013.

Author's Contribution

Publication I: "Determination of ^{235}U, ^{239}Pu, ^{240}Pu, and ^{241}Am in a Nuclear Bomb Particle Using a Position-Sensitive α-γ Coincidence Technique"

The author developed methods for analysing alpha-gamma coincidence data recorded in list mode. He also determined the efficiency calibrations of the detectors with Monte Carlo simulations, which were required for activity determination. In addition, he participated in the writing of the manuscript.

Publication II: "Advanced Alpha Spectrum Analysis Based on the Fitting and Covariance Analysis of Dependent Variables"

The author validated the statistical properties of the fitting and uncertainty estimation routines used in the ADAM alpha-particle spectrum analysis software. He also improved these routines, thereby increasing the reliability of the results. The author was the main contributor and had an active role in all phases of the work.

Publication III: "Determination of ^{239}Pu/^{240}Pu Isotopic Ratio by High-Resolution Alpha-Particle Spectrometry Using the ADAM Program"

The author contributed in finding the optimal procedures for the deconvolution of complex alpha-particle spectra with ADAM. He also identified the methods for uncertainty calculus and participated in the writing of the manuscript.

Publication IV: "Principles of UV–Gamma Coincidence Spectrometry"

The author is one of the inventors of the UV-gamma coincidence approach. He was the main contributor of this publication and had an active role in all phases of the work.

Publication V: "Fluorescence-Assisted Gamma Spectrometry for Surface Contamination Analysis"

The author participated in finding and investigating methods to increase the usability of the UV-gamma coincidence approach. He also derived the equations required to analyse coincidence spectra with a very low number of counts. He was the main contributor of the publication and had an active role in all phases of the work.

Publication VI: "^{140} La/^{140}Ba Ratio Dating of a Nuclear Release"

The author analysed gamma-ray spectra from air filters collected in Okinawa Japan in 2010 with AMUFI gamma spectrum analysis software. He used the spectra containing a clear signal of ^{140} La and ^{140}Ba to calculate an estimate for the date of a nuclear release. The author was the main contributor and had an active role in all phases of the work.

1. Introduction

Radioactive materials are necessary or even mandatory for numerous applications in research, medicine and industry, including energy production. However, these materials can also be hazardous through possible accidents or direct criminal acts against society [1, 2]. Nuclear materials are of special concern because of the risk of proliferation of nuclear weapons [3]. The key actions to prevent the adverse effects of the peaceful use of these materials are nuclear safety, security and safeguards (3S). Nuclear safety has the aim of protecting persons, property, society and the environment from accidental radiation hazards [4]. In nuclear security, the objective is the prevention of, detection of, and response to criminal or unauthorised acts [5]. Nuclear safeguards are measures to verify that states comply with their international obligations that material, facilities and information from peaceful nuclear activities are not diverted to the manufacture of nuclear weapons or other nuclear explosive devices [6].

Regardless of the progress in 3S, many problems have not yet been adequately solved and new challenges have also appeared during the last decade. The most dramatic reminder of the importance of nuclear safety was the Fukushima Dai-ichi nuclear disaster following an earthquake and tsunami in March 2011 in Japan. In the near future, decommissioning of nuclear facilities will be a major safety issue, as several facilities built in the 1960s and 1970s are reaching the end of their operational lifetime. The attacks of September 2001 in the United States raised the fear of radiological and nuclear terrorism. The threat of the criminal use of radioactive materials has since been recognised as a matter of grave concern. The murder of Alexander Litvinenko, a former officer of the Russian secret service, with radioactive polonium-210 in the United Kingdom in 2006 increased awareness of the use of radioactive materials as poisons against individuals [7]. In addition, the confirmed number

of illicit trafficking cases involving nuclear materials is alarming [8]. North Korean nuclear tests and the aspiration for uranium enrichment in Iran have highlighted the importance of nuclear arms control to prevent further proliferation.

The control of nuclear and other radioactive materials is not only a matter of political decisions but also a question of the availability of technical solutions. Practical implementation requires the development of novel approaches to verify the compliance of declared activities and especially to detect and identify unknown activities. For example, the monitoring regime of the Comprehensive Nuclear-Test-Ban Treaty (CTBT) consists of a network of radionuclide, seismic, infrasound and hydroacoustic stations around the world to detect traces of nuclear explosions [9, 10, 11, 12, 13]. Verification of the treaty on the Non-Proliferation of Nuclear Weapons (NPT) is also a great technological challenge. Safeguards by the International Atomic Energy Agency (IAEA) require a range of techniques to ensure that materials or know-how from the peaceful use of nuclear energy is not diverted to nuclear weapons [14]. To support the process of arms control and disarmament, the scientific and technological basis must be established [15]. Nuclear and radiological terrorism is a new threat, and methods for its prevention remain permanently on the international security agenda [16].

1.1 Characterisation of nuclear material

An ideal method for the characterisation of nuclear and other radioactive materials would provide high sensitivity and precision in a reasonable time. In addition, the analysis method should be non-destructive, ensuring that the results can later be confirmed with complementary methods. Chemical separation of the elements should be postponed as long as possible, both for simplicity and to keep the sample intact. Methods suitable for on-site analysis are the most favourable, since the transportation of samples to the laboratory is often time consuming. The handling of multiple samples of different origin in the same laboratory also increases the risk of cross-contamination.

In practice, the range of techniques available compromises these requirements [14, 17, 18]. Mass spectrometry provides the highest sensitivity and precision, e.g. for the analyses of plutonium, uranium and other long-lived nuclides. Unfortunately, mass spectrometers require la-

borious sample preparation processes or are large and expensive. Therefore, they are only available in dedicated laboratories. Radiometric techniques identifying nuclides based on the radiation emitted in radioactive decay are significantly simpler and less expensive. Options include alpha-particle, beta-particle, gamma-ray, conversion electron and neutron counting. Among these, the most frequently employed and relevant to this work are gamma-ray and alpha-particle spectrometry.

Gamma-ray spectrometry is the most mature and widely used nuclear analysis method for several reasons. First, gamma rays are emitted at discrete energies unique for each nuclide. Thus, the nuclide can be identified based on the detected gamma-ray energy spectrum. Second, gamma rays are photons with a typical energy above 100 keV. Unlike charged particles, these photons have a finite probability of passing through matter without any interaction. In particular, the absorption of high-energy gamma rays in media is weak. Therefore, sample preparation is typically not required and the analysis can be performed non-destructively. In-situ gamma-ray measurements allow the detection and identification of sources over long distances and even behind shields.

On the other hand, transuranium and other heavy nuclides decaying by alpha-particle emission are often difficult to detect with gamma-ray spectrometry. The decay of these nuclides produces few gamma rays, because deexcitations of the excited states take place via the emission of conversion electrons instead of gamma rays. If gamma rays are produced, they typically have energies from 10 to 100 keV (see Table 1.1). The small number of low-energy photons is easily absorbed in the material between the source and the detector.

The use of gamma-ray spectrometry is also restricted by background radiation and difficulties in the analysis of complex spectra. The background arises from natural radioactivity in the detector environment, including cosmic radiation, and from other radionuclides in the sample. Since gamma rays are highly penetrating, shielding the measurement setup from external radiation is difficult, limiting the detection of small activities. In spectrum analyses, efficient methods are required to detect small signals above the background, and especially to distinguish between isotopes having emission energies so close to each other that they overlap in the recorded spectrum.

Alpha-particle spectrometry characterises radionuclides based on the helium nuclide emitted in the decay. These so-called alpha particles have

Table 1.1. Nuclides typically quantified with alpha-particle spectrometry in significantly lower concentrations than with gamma-ray spectrometry. The alpha-particle energies refer to the most intense emission and yields to the total alpha-particle branching. Gamma-ray energies and yields refer to the most dominant gamma-ray transition.

Nuclide	α energy (keV)	α yield (%)	γ energy (keV)	γ yield (%)
^{238}Pu	5499	100	43.50	0.039
^{239}Pu	5157	100	51.62	0.027
^{240}Pu	5168	100	45.24	0.045
^{242}Pu	4902	100	44.92	0.035
^{235}U	4398	100	185.71	57.2
^{238}U	4198	100	49.55	0.064
^{210}Po	4517	100	803.06	0.0010
^{241}Am	5486	100	59.54	35.9

nuclide-specific discrete energies ranging from 3 to 10 MeV. The advantages of alpha-particle measurements are the negligible background and very high intrinsic detection efficiency (close to one). Many heavy nuclides decaying by alpha-particle emission can be quantified with alpha-particle spectrometry in significantly lower concentrations than with gamma-ray spectrometry.

Unfortunately, the high stopping power of alpha particles in matter complicates the analysis. Alpha particles emitted by radioisotopes travel only a few centimetres in air [19]. Therefore, the alpha-particle detector must be brought into immediate contact with the source or the measurement must be performed in a vacuum. Also, alpha particles cannot be measured through any packing or shield. The prevention of absorption in the sample matrix requires destructive sample preparation. A thick, poorly-prepared sample produces a spectrum with peaks extensively tailing to lower energies, complicating the analysis of nuclides having alpha-particle energies close to each other. Some nuclides, such as ^{239}Pu and ^{240}Pu, are difficult to distinguish even after careful sample preparation. Advanced spectrum deconvolution methods are required to analyse alpha-particle spectra consisting of multiple overlapping peaks.

1.2 Objectives of the work

The objective of this thesis was to improve the rapid characterisation of nuclear and other radioactive materials. The work concentrated

on novel measurement techniques and spectrum analysis approaches for radiometric methods. The research problem was divided into two questions:

1. *How can statistical uncertainties be taken into account correctly in spectrum analysis?*
   Obtaining correct uncertainty estimates for parameters from spectrum analysis is crucial for the reliable interpretation of the results. Unfortunately, the methods commonly used in spectrum analysis underestimate the uncertainties of overlapping peaks. Here, new analysis software utilising covariance calculus for uncertainty estimation is introduced for the analysis of gamma-ray spectra in Chapter 3 and alpha-particle spectra in Chapter 4. The chapters are based on three publications. The reliability of the uncertainty estimation method was extensively tested in Publication II. In Publications III and VI, the software was applied to the analysis of practical problems in alpha-particle and gamma-ray spectrometry, respectively.

2. *What extra information can alpha-gamma coincidence measurements provide compared to separate measurements?*
   In an alpha-gamma coincidence measurement, alpha particles and gamma rays originating from the same decay are simultaneously detected. The technique has the potential to provide an efficient approach to reduce the background disturbing the analysis of nuclear materials using gamma-ray spectrometry. The capabilities of the technique by using a combination of traditional alpha-particle and gamma-ray spectrometers are discussed in Chapter 5 of this thesis and in Publication I. For the first time, the coincidence technique has also been extended to the stand-off analysis of alpha-particle-emitting radionuclides by using secondary UV radiation produced in the alpha-particle absorption in air. This UV-gamma approach presented in Publications IV and V is discussed in Chapter 6.

The two research topics are also tightly interrelated. For example, simple alpha-particle measurement followed by complex spectrum analysis with multiple overlapping peaks competes with the more demanding alpha-gamma coincidence measurement resulting in a simple spectrum. The optimal approach depends on the isotopes present, measure-

ment time, as well as on the sample and measurement geometries. Moreover, in the analysis of coincidence spectra with a very low background, the smallest detectable peaks may contain only a few counts. This makes the analyses sensitive to any shortcoming in the software.

In all analysis, special emphasis has been placed on the statistics. Therefore, the statistical methods used are described in detail in Chapter 2.

2. Statistical methods

The randomness arising from the inherent stochastic nature of radioactive decay is always present. Therefore, the number of events detected in a particular radiation measurement cannot be accurately predicted, and repeated measurements lead to different outcomes.

The goal of this chapter is to describe essential methods to draw conclusions on radiation measurements, taking the stochastic variations of the measurement quantities into account. The methods presented are required to accomplish the analysis utilised in other parts of this thesis. A particular emphasis is placed on two topics commonly ignored when analysing radiation energy spectra. The first topic is how to calculate the detection limit if the number of detected counts is too small to be approximated by the Gaussian distribution. The second topic is how to obtain uncertainty limits for correlated parameters in spectrum fitting and how to take the correlation into account in the further interpretation of the results.

2.1 Limit of detectability

A common question in the analysis of radiation measurements is to decide whether the detected signal is caused by the radionuclide of interest or by the statistical variation of the background. This question is typically evaluated through two parameters defined by Lloyd Currie in 1968 [20]. The critical level (L_C) is the minimum number of counts above the background considered as a real signal. Taking the detection decision at a level L_C leads to the risk of a false detection with probability P_α. Given this critical level, the limit of detection (L_D) is the mean true signal not detected with probability P_β. L_D can be further used to calculate the minimum detectable activity (MDA) by combining the value with the

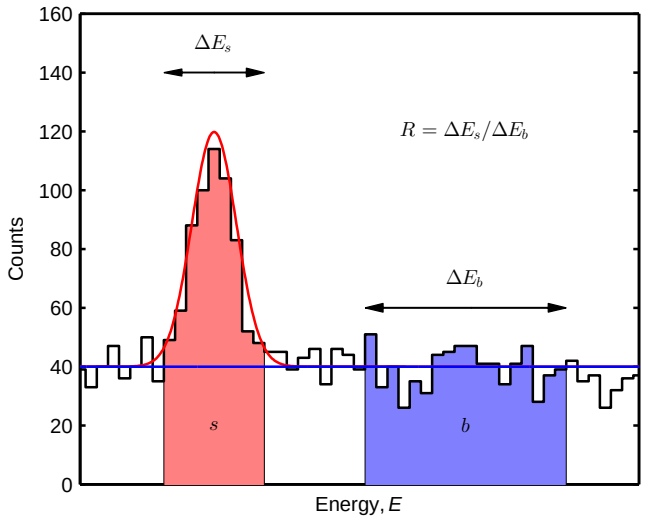

Figure 2.1. Example of a spectrum where the energy range ΔE_s is used as a signal region and the energy range ΔE_b as a background region. The shaded areas represent the number of counts (s and b) in these regions. The background level is considered to be independent of energy.

detection efficiency ε, measurement time t and radiation yield y:

$$\mathrm{MDA} = \frac{1}{\varepsilon t y} L_D. \tag{2.1}$$

To calculate L_C and L_D for specific risk levels, the number of background counts must be estimated. The estimate is typically based on the number of counts in a separate blank measurement or on the number of counts in an energy region adjacent to the region of interest in the same measurement (see Figure 2.1). In both cases, the mean number of counts in the region of interest when no real signal is present (μ_0) is considered to be directly proportional to the mean number of counts in the background region (μ_b):

$$\mu_0 = R\mu_b. \tag{2.2}$$

The constant R takes into account factors such as the difference in the acquisition time between the signal and background measurement or the difference between the width of the two energy regions.

To facilitate the reading of this section, the definitions of the most important notations have been collected in Table 2.1.

Gaussian approach Currie derived the equations for L_C and L_D in a case where the variations in both the background and in the signal can be approximated to be Gaussian[1]:

$$L_C = k_\alpha \sqrt{Rb(1+R)}, \tag{2.3}$$

[1]Often, a notation $L_C = k_\alpha \sqrt{B(1+1/m)}$ is used, where $B = Rb$ and $m = 1/R$.

Table 2.1. Definition of notations used in Section 2.1.

Notation	Definition
b	Detected number of counts in background region
μ_b	Mean number of counts in background region
s	Detected number of counts in signal region
μ_0	Mean number of counts in signal region when no real signal is present
R	Ratio μ_0/μ_b
L_C	Critical level
T_D	Detection threshold
L_D	Limit of detection
P_α	False detection probability (false positive)
P_β	False rejection probability (false negative)
MDA	Minimum detectable activity

$$L_D = L_C + \frac{k_\beta^2}{2}\left(1 + \sqrt{1 + \frac{4}{k_\beta^2}\left(L_C + \left(\frac{L_C}{k_\alpha}\right)^2\right)}\right). \tag{2.4}$$

Here, b is the detected number of background counts. k_α and k_β denote abscissas of the standard normal distribution corresponding to probabilities $1 - P_\alpha$ and $1 - P_\beta$. The minimum total number of counts in the region of interest considered as detection is defined by the detection threshold T_D:

$$T_D = L_C + Rb. \tag{2.5}$$

Figure 2.2 illustrates the relationships between b, P_α, T_D, P_β and L_D.

Poisson approach The concept of detection limit is also useful for applications where the Gaussian approximation is not valid. Especially in coincidence measurements discussed in Chapter 5 and 6, the background level can be very small ($R\mu_b << 1$). In the most extreme case, one count can already be considered as a sufficiently firm indication of a signal.

Here, formulae for T_D and L_D are derived directly from the probability mass function of the Poisson distribution, which is valid even if the number of counts is very low. Similar equations have previously been presented in References [21, 22]. However, the equations presented here are derived independently and the formula obtained for L_D differs slightly from the one suggested in the references. In addition, the derivations of the equations are not explicitly shown in the references.

Bayesian interference is used in deriving the equations for T_D and L_D. Assuming a mean number of counts μ_c, the probability of detecting c

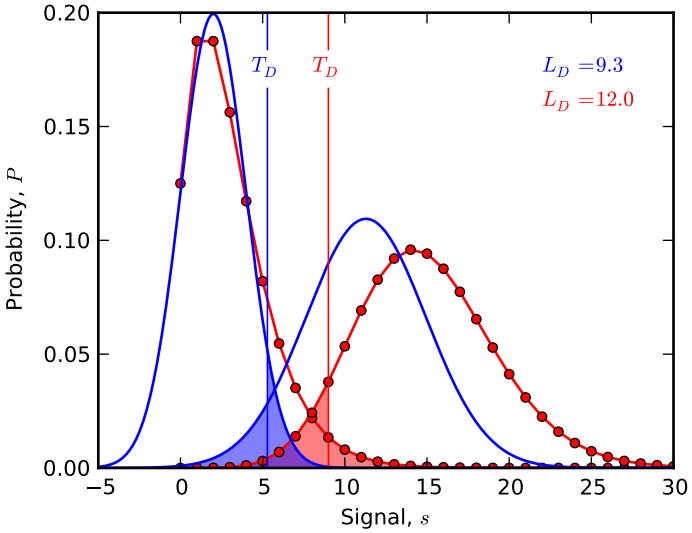

Figure 2.2. Probability mass functions based on the Poisson statistics (red) and probability density functions based on the Gaussian statistics (blue) of the detected signal s, when $b = 2$, $R = 1.0$. The mean signal produced by the source is either 0 or L_D. The vertical lines represent the value of T_D, and the shaded areas the probabilities (P_α and P_β), which are set to 0.05.

counts is

$$P(c|\mu_c) = P_{\text{Pois}}(c;\mu_c), \tag{2.6}$$

where $P_{\text{Pois}}(c;\mu_c)$ is the probability mass function of the Poisson distribution:

$$P_{\text{Pois}}(c;\mu_c) = \frac{\mu_c^c}{c!}\exp(-\mu_c). \tag{2.7}$$

By using Bayes' rule with uniform prior ($P(\mu_c) = 1$), it can be seen that the likelihood $P(\mu_c|c)$ results in the same form:

$$P(\mu_c|c) = \frac{P(c|\mu_c)P(\mu_c)}{\int_0^\infty P(c|\mu_c)P(\mu_c)\mathrm{d}\mu_c} = P_{\text{Pois}}(c;\mu_c). \tag{2.8}$$

Well-known background

Let us first have a look at a simple case where the mean background (μ_b) is considered to be known. When no real signal is present, the probability of detecting s counts in the region of interest is obtained from Equations 2.2 and 2.6:

$$P(s|\mu_0) = P_{\text{Pois}}(s;R\mu_b) = \frac{(R\mu_b)^s}{s!}\exp(-R\mu_b). \tag{2.9}$$

P_α is the summed probability of all cases having the number of counts in the signal region equal to or above the selected detection threshold T_D when no real signal is present:

$$P_\alpha = \sum_{s=T_D}^{\infty} P(s|\mu_0) = 1 - \sum_{s=0}^{T_D-1} \frac{(R\mu_b)^s}{s!}\exp(-R\mu_b). \tag{2.10}$$

P_β is calculated to correspond to a selected true signal producing on average L_D counts in the signal region. It is the summed probability of all cases having a number of counts in the signal region below the selected T_D:

$$P_\beta = \sum_{s=0}^{T_D-1} P(s|L_D + \mu_0) = \sum_{s=0}^{T_D-1} \frac{(L_D + R\mu_b)^s}{s!} \exp(-L_D - R\mu_b). \tag{2.11}$$

Measured background

If the mean background is not precisely known, calculation of T_D and L_C becomes more challenging. Now, the probability of detecting s counts in the signal domain is obtained from the prior predictive distribution:

$$P(s|b; R) = \int_0^\infty P(s|R\mu_b)P(\mu_b|b)\mathrm{d}\mu_b. \tag{2.12}$$

The conditional probabilities in the case of the Poisson distribution have been defined in Equations 2.6 and 2.8.

Again, P_α is the summed probability of all cases having the number of counts in the signal region equal to or above T_D:

$$\begin{aligned} P_\alpha &= \sum_{s=T_D}^{\infty} P(s|b; R) \\ &= 1 - \sum_{s=0}^{T_D-1} \frac{1}{b!s!} \frac{R^s}{(1+R)^{b+s+1}} \Gamma(b+s+1) \\ &= 1 - \sum_{s=0}^{T_D-1} \binom{b+s}{s} \frac{R^s}{(1+R)^{b+s+1}}. \end{aligned} \tag{2.13}$$

The equation has been simplified by using the definition of a Gamma function:

$$\Gamma(n) = \int_0^\infty t^{n-1}e^{-t}\mathrm{d}t = (n-1)!. \tag{2.14}$$

Likewise,

$$P(s|b; R, L_D) = \int_0^\infty P(s|L_D + R\mu_b)P(\mu_b|b)\mathrm{d}\mu_b \tag{2.15}$$

and

$$\begin{aligned} P_\beta &= \sum_{s=0}^{T_D-1} P(s|b; R, L_D) \\ &= \sum_{s=0}^{T_D-1} \int_0^\infty \frac{(L_D + R\mu_b)^s}{s!} e^{-(L_D+R\mu_b)} \frac{\mu_b^b}{b!} e^{-\mu_b} \mathrm{d}\mu_b. \end{aligned} \tag{2.16}$$

In a typical case, the values of T_D and L_D are calculated to refer to the selected probabilities P_α and P_β. In the Poisson approach, the values for

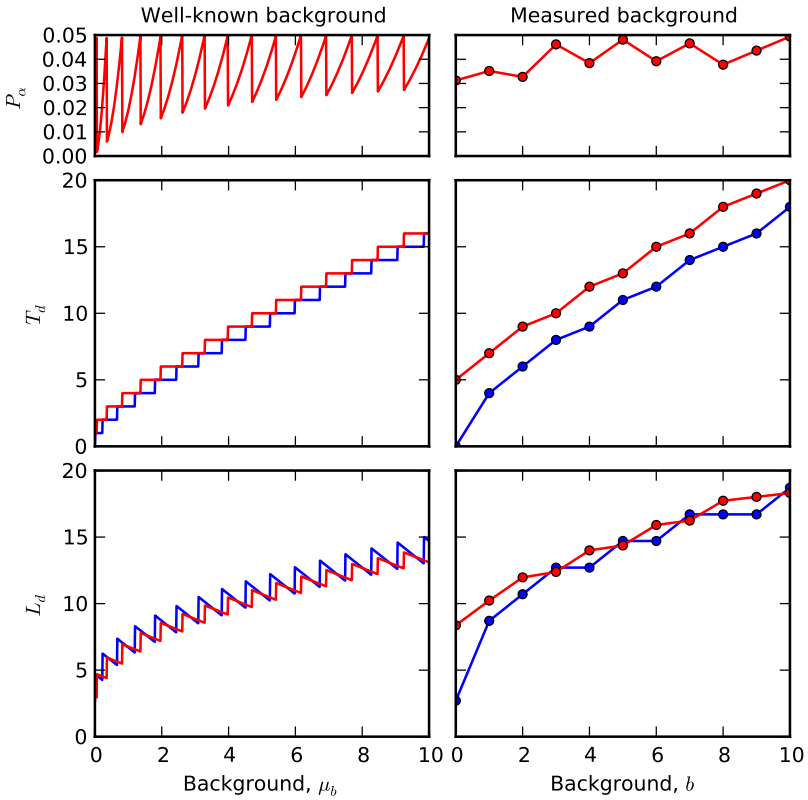

Figure 2.3. Detection threshold (T_D) and limit of detection (L_D) as a function of a well-known (left) or measured (right) background (μ_b or b). The values are calculated based on both the Poisson (red) and Gaussian (blue) statistics. The constant R is set to 1.0, and both probabilities (P_α and P_β) to 0.05. The Gaussian T_D's have been rounded up to the nearest integer. The corresponding exact P_α probabilities according to the Poisson statistics are also shown.

T_D and L_D must be determined iteratively. In addition, since the number of detected counts in Poisson statistics is discrete, the selected value for P_α cannot be exactly reached. Instead, the number of counts corresponding to the closest values below the selected P_α should be used.

The limits of detectability based on the Poisson and Gaussian statistics are compared in Figures 2.2 and 2.3. As can be seen from Figure 2.3, the Gaussian and Poisson statistics result in similar values for T_D and L_D if the background is well known. Instead, for measured background consisting of only a few counts, the use of the Gaussian statistics may lead to a significant underestimation of both T_D and L_D. The difference between the Gaussian and Poisson approach diminishes when the number of detected background counts increases. Based on the probability mass functions compared in Figure 2.2, the difference between these two approaches also depends on the selected probabilities P_α and P_β, and is most pronounced for small probabilities.

The formulae for the limit of detectability based on the Poisson statistics are utilised for MDA calculus in Section 6.2 and Publication V of the present thesis. In contrast, the analysis in Section 5.3 and Publication I rely on the traditional Gaussian approach[2]. However, the main conclusions of the studies do not depend on which model was used to calculate the MDA.

2.2 Fitting

This section presents a method based on covariance calculus to fit a non-linear model to data points. The objective is to resolve the best estimates for the unknown parameters of the function and also the uncertainties of the estimates. The method discussed is a standard procedure presented in many textbooks dealing with data analysis (see, for example, Reference [23]). It is valid for data points following a Gaussian distribution.

In this thesis, the method has been applied to the analysis of gamma-ray spectra (Publication VI and Chapter 3) and alpha-particle spectra (Publications II, III and Chapter 4). Therefore, the data set is assumed to be a measured energy spectrum consisting of successive channels with a certain number of counts. The number of counts in each channel is expected to be large enough to follow a Gaussian distribution approximately.

The maximum likelihood estimate for the unknown parameters is obtained with the weighted least-squares method. In this approach, the optimum is reached when the weighted sum, S, of the squared residuals of the counts in channels is minimised. The function for S can be expressed either as a sum or in a matrix form:

$$S = \sum_{n=1}^{N} w_n (y_n - f_n)^2 = (\boldsymbol{y} - \boldsymbol{f})^{\mathrm{T}} \boldsymbol{W} (\boldsymbol{y} - \boldsymbol{f}). \tag{2.17}$$

Here, $\boldsymbol{y}$ and $\boldsymbol{f}$ are vectors containing the measured and modelled numbers of counts in each channel, respectively. The value of the function f in channel n depends on free ($\boldsymbol{\beta}$) and constant ($\boldsymbol{c}$) parameters. The elements w_n of the weight matrix $\boldsymbol{W}$ are equal to the reciprocal of the covariances of the counts in different channels. Since the errors in the counts are

[2]At the time when Publication I was written, the precise equations based on the Poisson statistics had not yet been derived.

uncorrelated, the weight matrix is diagonal:

$$\boldsymbol{W} = \mathrm{diag}[\sigma_1^{-2} \cdots \sigma_n^{-2}]. \tag{2.18}$$

If function f is linear with respect to all unknown parameters $\boldsymbol{\beta}$, Equation 2.17 becomes an ordinary least-squares problem with a closed-form solution. In contrast, the non-linear problem has no closed-form solution, and it must be solved by iterative refinement. A simple approach is to use the Gauss-Newton algorithm, which approximates the system by a linear function at each iteration. $\boldsymbol{f}$ is linearised by using a first-order Taylor series expansion:

$$\boldsymbol{f}^{k+1} \approx \boldsymbol{f}^k + \boldsymbol{J}(\boldsymbol{\beta}^{k+1} - \boldsymbol{\beta}^k). \tag{2.19}$$

Here, $\boldsymbol{f}^k$ and $\boldsymbol{\beta}^k$ are the function and parameter values from the previous iteration k. $\boldsymbol{J}$ is a Jacobian matrix of $\boldsymbol{f}$ with parameter values $\boldsymbol{\beta}^k$. The elements of the matrix are defined as

$$J_{nm} = \frac{\partial f_n(\boldsymbol{\beta}^k, \boldsymbol{c})}{\partial \beta_m}, \tag{2.20}$$

where index m goes over the free parameter and n over the channels.

A new estimate for the parameter values is calculated by inserting $\boldsymbol{f}$ from Equation 2.19 into Equation 2.17 and minimising S with respect to $\boldsymbol{\beta^{k+1}}$:

$$(\boldsymbol{\beta}^{k+1} - \boldsymbol{\beta}^k) = (\boldsymbol{J}^{\mathrm{T}}\boldsymbol{W}\boldsymbol{J})^{-1}\boldsymbol{J}^{\mathrm{T}}\boldsymbol{W}(\boldsymbol{y} - \boldsymbol{f}^k). \tag{2.21}$$

For the first fit, the initial parameter values $\boldsymbol{\beta}_0$ are given by the user. The derivatives $\boldsymbol{J}$ can either be solved analytically or approximated numerically according to the equation

$$J_{nm} = \frac{f_n(\boldsymbol{\beta} + \boldsymbol{\Delta}_m, \boldsymbol{c}) - f_n(\boldsymbol{\beta}, \boldsymbol{c})}{\|\boldsymbol{\Delta}_m\|}, \tag{2.22}$$

where $\boldsymbol{\Delta}_m$ is a small deviation from β_m.

The iterative process is repeated until the value of $\boldsymbol{\beta}$ has converged. The converged value is the estimate $\tilde{\boldsymbol{\beta}}$. Estimates for the uncertainties of the fitted parameters are obtained from the covariance matrix:

$$\boldsymbol{\sigma}^2(\tilde{\boldsymbol{\beta}}) = (\boldsymbol{J}^{\mathrm{T}}\boldsymbol{W}\boldsymbol{J})^{-1}. \tag{2.23}$$

The variances of the parameters lie on the diagonal axis of the matrix. Generally, these parameter values are correlated. The off-diagonal elements contain the covariances between the parameters.

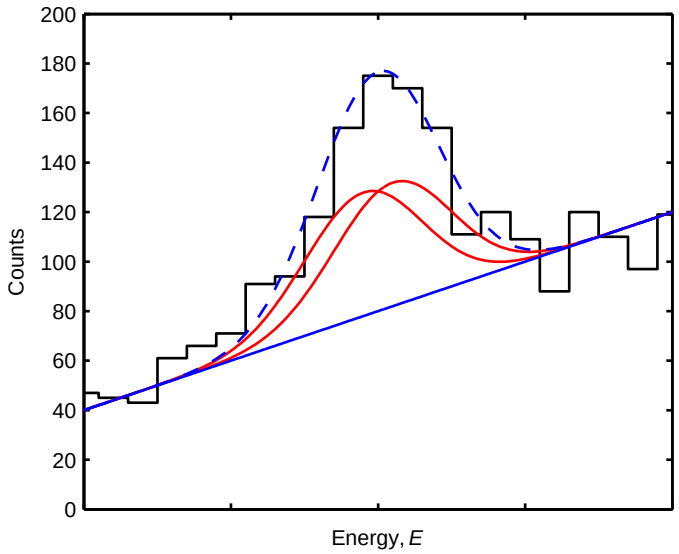

Figure 2.4. Part of a simulated gamma-ray spectrum with two overlapping peaks. The correlation between the fitted peak areas is notable, i.e., they compete for the same counts. The dashed blue line shows the total fit.

2.3 Combined uncertainty of dependent variables

This section presents a brief overview of the uncertainty estimation of dependent variables. In data analysis, correlations between variables are often neglected and all variables are treated as independent. However, the correlations must be taken into account to determine the combined uncertainty of a measurand calculated from input quantities. Neglecting the correlations of the input quantities may lead to a significant underestimation or overestimation of the combined uncertainty. The treatment of uncertainties is discussed in detail in References [24, 25].

In spectrum analysis, several parameters depend on each other. For example, the peak and baseline areas are often correlated. Correlations between different peak-shape parameters are also common. For overlapping peaks close to each other, the negative correlation between the peak areas is especially notable (see Figure 2.4). Due to the correlation, the summed area of the peaks can be determined precisely, even though the uncertainties of the individual peaks areas are large: The area of one peak being possibly too small is compensated by the increased area of the other.

To study the influence of correlation, let us define a quantity Y that is not measured directly but is determined from N input quantities X_1, X_1, $\ldots X_N$ through a function f:

$$Y = f(X_1, X_2, \ldots, X_N). \tag{2.24}$$

The uncertainty $u(x_i)$ of an estimated value x_i of the input quantity X_i is characterised by its variance ($u^2(x_i) = \sigma^2(x_i)$). For simplicity, the input quantities are expected to follow a Gaussian distribution.

When Y can be expressed as a linear combination of the input quantities X_i, the combined uncertainty follows from the basic properties of variance:

$$Y = f(X_1, X_2, \ldots, X_N) = \sum_{i=1}^{N} A_i X_i \tag{2.25}$$

$$\begin{aligned} u^2(y) = \sigma^2(y) &= \sum_{i=1}^{N}\sum_{j=1}^{N} A_i A_j \sigma(x_i, x_j) \\ &= \sum_{i=1}^{N} A_i^2 \sigma^2(x_i) + 2\sum_{i=1}^{N-1}\sum_{j=i+1}^{N} A_i A_j \sigma(x_i, x_j). \end{aligned} \tag{2.26}$$

Here, A_i is a well-known constant. The variance $\sigma^2(x_i)$ and covariance $\sigma(x_i, x_j)$ are defined through the expectation value E:

$$\sigma^2(x_i) = \sigma(x_i, x_i) = \mathrm{E}\left[(x_i - \mathrm{E}(x_i))^2\right] \tag{2.27}$$

$$\sigma(x_i, x_j) = \mathrm{E}\left[(x_i - \mathrm{E}(x_i))\,(x_j - \mathrm{E}(x_j))\right]. \tag{2.28}$$

The individual variances set the minimum and maximum limits for the covariance of any two variables:

$$\min(\sigma(x_i, x_j)) = -\sigma(x_i)\sigma(x_j) \qquad \max(\sigma(x_i, x_j)) = \sigma(x_i)\sigma(x_j). \tag{2.29}$$

The minimum value corresponds to a perfect negative correlation and the maximum value to a perfect positive correlation. For uncorrelated variables, the covariance is zero.

When Y is defined through an arbitrary non-linear function $f(X_1, X_2, \ldots, X_N)$, the estimated values y do not follow a Gaussian distribution. However, if f is only weakly non-linear, the function can be approximated with a first-order Taylor expansion. In this case, the uncertainty can be estimated from Equation 2.26 calculated for the linearised function:

$$\begin{aligned} u^2(y) &= \sum_{i=1}^{N}\sum_{j=1}^{N} \frac{\partial f}{\partial x_i}\frac{\partial f}{\partial x_j}\sigma(x_i, x_j) \\ &= \sum_{i=1}^{N} \left(\frac{\partial f}{\partial x_i}\right)^2 \sigma^2(x_i) + 2\sum_{i=1}^{N-1}\sum_{j=i+1}^{N} \frac{\partial f}{\partial x_i}\frac{\partial f}{\partial x_j}\sigma(x_i, x_j). \end{aligned} \tag{2.30}$$

Ratio of two variables For this thesis, the combined uncertainty of the ratio of two variables is especially relevant, since it has been utilised in Publications III and VI. The combined uncertainty of the ratio of correlated variables X_1 and X_2 can be estimated starting from Equation 2.30:

$$Y = f(X_1, X_2) = \frac{X_1}{X_2} \tag{2.31}$$

$$u^2(y) = \frac{1}{x_2}\sigma^2(x_1) + \frac{x_1}{x_2^2}\sigma^2(x_2) - 2\frac{x_1}{x_2^3}\sigma(x_1, x_2). \tag{2.32}$$

It should be noted that the function f is highly non-linear when x_2 approaches zero. Strictly speaking, the ratio of two normally distributed variables does not follow a Gaussian but a generalised Cauchy distribution [26]. For this distribution, the variance is undefined and the confidence limits need to be calculated with Filler's theorem [27]. However, Equation 2.32 is still applicable if the estimates of the input quantities are far from zero ($|x_1/\sigma(x_1)| >> 1$ and $|x_2/\sigma(x_2)| >> 1$).

2.4 Conclusions

The limit of detectability for radiation measurements can be calculated solely based on the Poisson statistics. Since no Gaussian approximation was utilised to derive the presented formulae, they are valid even if the number of detected counts remains small. It was shown that the Gaussian approximation commonly used may lead to a serious underestimation of the detection threshold, causing an undesired large probability for false detection. The underestimation becomes significant when the measured background falls below ten counts. However, the difference also depends on the desired false detection probability. By using only the Poisson statistics, the calculus becomes computationally more intense. Therefore, the simpler approach relying on the Gaussian approximation is often feasible provided that the underlying presumptions have a sound statistical basis.

The new algorithms for spectrum analysis offer a straightforward means for taking into account the correlations between the fitted parameters. The fitting routine yields both the variances and covariances of the fitted parameters. These, in turn, are required to estimate the combined uncertainty of a measurand calculated from these parameters.

Omitting the covariances may lead to a significant underestimation or overestimation of the combined uncertainty.

It is important to notice that in the derivation of the fitting routine, the Gaussian approximation was used. Thus, the method cannot be directly applied for the analysis of spectra consisting of only a small number of counts (see Section 3.2). However, with a few simple modifications, the feasible range of the fitting method can be greatly extended. These modifications are presented in Chapter 4 together with the results obtained by analysing alpha-particle spectra with only a few counts.

3. Analysis of gamma-ray spectra

Gamma-ray detectors are widely used for the detection and characterisation of radioactive materials both in laboratory and field applications. In radioanalytical laboratories, measurements are commonly performed with a high-purity germanium detector (HPGe) inside a lead shield. The germanium detectors are cooled either electrically or with liquid nitrogen, and they offer an excellent energy resolution (FWHM ~0.2% at 662 keV), helping to distinguish between isotopes having gamma-ray emission energies close to each other. Even better energy resolution is obtained with micro calorimeters [28]. However, micro calorimeters are currently mainly used in basic research and they require extensive cooling to near absolute zero. In field applications, scintillation detectors operating at room temperature are most common. Sodium iodide (NaI) scintillators with a large volume enable a high detection efficiency for an affordable price. However, the energy resolution of these detectors is relatively poor (FWHM above 6%). Lanthanum bromide ($LaBr_3$) scintillators have a considerably better energy resolution (below 3%) compared to NaI, but they are also significantly more expensive, especially in large sizes [29]. Strontium iodide (SrI_2) is a promising scintillator material that may supersede $LaBr_3$ in the future [30]. Of the room-temperature semiconductor detector materials, cadmium zinc telluride (CdZnTe) provides a pleasing resolution below 2% [31, 32]. Unfortunately, the crystal cannot be grown to larger than about 1 cm^3.

For the analysis of the recorded gamma-ray spectra, a large variety of software packages exist today, including UniSampo [33], Genie [34], GammaVision [35] and Aatami [36]. They are largely based on the same principles already utilised in the first computer-based analysis software for gamma-ray spectra presented in the 1960s [37]. The methods rely on the fitting of the full-energy photo peaks above a continuous baseline.

These photo peaks consist of gamma rays that have reached the detector without prior interaction and released all of their energy there.

A common limitation of commercial spectrum analysis software is the insufficient uncertainty estimation of the fitted parameters. In the IAEA intercomparison of gamma-ray analysis software in 1998 and 2002, the programs exhibited reasonable statistical control in the analysis of singles peaks on a smooth baseline [38, 34]. However, all programs underestimated the peak area uncertainties in the analysis of two overlapping peaks. The programs estimate the uncertainties based on the peak and background area in the vicinity of the peak [39]. These heuristic methods for uncertainty calculus cannot handle competing parameters arising from peak multiples or peaks residing on a nonlinear background. Even though the intercomparison results are quite old, the basis of the uncertainty estimation routines in several codes has not been changed. In this thesis, the problem with the reliability of the uncertainty estimation is solved by using full covariance calculus of all fitted parameters (see Section 2.2).

The statistical control lacking in the commercial codes becomes especially crucial in the fully automated analysis of large numbers of spectra. Since the manual rejection of false alarms is a tedious task, the software must comply with the selected false alarm rate. In nuclear security, the tolerated false alarm rate can be as low as one per thousand or even one per million measurements. The methods for uncertainty estimation are emphasised in the analysis of low-resolution NaI- or $LaBr_3$-scintillator spectra, which often contain multiple overlapping peaks and complex baseline shapes.

3.1 AMUFI analysis software

The AMUFI[1] (Advanced Multiplet fitting) spectrum analysis software has been especially designed for the fully automated analysis of large number of spectra. AMUFI is run on the command line and the analysis is controlled with an XML parameters file. Graphical tools are provided for parameter file creation and for viewing results. The analysis procedure

[1] AMUFI was coded for STUK in 2010-2013 by Andreas Pelikan, Dienstleitungen in der automatischen Datenverarbeitung und Informationstechnik, Austria. Other people contributing to the development of the software are Harri Toivonen (project management and software architecture) and Sakari Ihantola (algorithms and testing).

is based on hypothesis testing where predefined shapes are fitted to the spectrum.

Rather than making yet another complete toolkit for gamma-ray spectrometry, the vision in the development of AMUFI has been to create a selection of software programs, each optimised for a single task. This modular structure allows the flexible use of the code. The different components are linked together via a LINSSI database [40]. AMUFI itself only takes care of spectrum fitting. The software reads the spectrum, calibrations and possible shape components from a database. The input data can be generated with any software supporting the LINSSI format. Analysis results are also saved into LINSSI, where they can be viewed, for example, with the LINSSI web interface or a dedicated report generator.

Spectrum shapes AMUFI deploys three types of shapes for spectrum deconvolution (f_g, f_b and S). f_g and f_b are analytical functions describing the full energy absorption peak and baseline, respectively. S is an arbitrary, complete spectral shape, which can be based either on a measurement or simulation.

The analytical functions are for direct analysis of unambiguous shapes. To minimise the number of parameters, the functions are simpler than in many other spectrum analysis programs. The model for the photo peak f_g is a Gaussian function:

$$f_g(E; E_p) = \frac{1}{\sqrt{2\pi\sigma^2}} \exp\left(-\frac{(E-E_p)^2}{2\sigma^2}\right). \tag{3.1}$$

Here, E denotes the energy of the channel and E_p the nominal energy of the peak. The shape parameter of the Gaussian function (σ) depends on the detector resolution (FWHM $= 2.355\sigma$). The baseline function f_b is a straight line defined by parameters C_0 and C_1:

$$f_b(E; C_0, C_1) = C_0 + C_1 E. \tag{3.2}$$

Complex shapes that cannot be adequately described with these analytical functions are taken into account with model S. Typically, S is a non-linear baseline shape obtained from a separate blank measurement. It may also be either a measured or simulated full nuclide response including not only the photo peak but also the scattered component. The statistical variations of the measured responses can be reduced with successive smoothing and multiplicative bias correction [41].

Calibration In the analysis of gamma-ray spectra, the energy and resolution calibration parameters do not depend on the measurement

geometry. Also, the shape of the efficiency calibration is not very sensitive to small variations in the geometry. Therefore, AMUFI uses fixed, measurement-setup specific calibration parameters read from a database.

All calibration parameters in gamma-ray spectrometry are dependent on energy. In particular, the precise energy dependence of efficiency is relatively complex. Furthermore, the dependence between the absorbed energy and recorded channel is often somewhat nonlinear. Therefore, AMUFI supports several different functions for resolution, efficiency and energy calibration. The resolution and energy calibration can often be extracted directly from the peaks in the measured spectrum with a calibration management program. The efficiency calibration is typically based on a separate calibration measurement or Monte Carlo simulation.

Fitting In AMUFI, the fitting and peak-area uncertainties are based on covariance calculus discussed in Section 2.2. The basic fitting parameters are the nuclide raw activity, baseline and spectral shape components.

For the analysis, the spectrum is divided into fitting regions analysed independently by default. Inside each fitting region, all peaks originating from the same nuclide reflect its activity. That is, the peak areas are not free fitting parameters but are tied to the activity through the efficiency calibration and nuclear data. The peak energies are also read from the nuclear data. The fitting model for a region consisting of N nuclides having M_n peaks is

$$f(E) = t\left[\sum_{n=1}^{N} a_n \sum_{m=1}^{M_n} y_m \varepsilon(E_{p,m}) f_g(E, E_{p,m}) + f_b(E; C_0, C_1) + \sum_{k=1}^{K} D_k S_k(E)\right]. \tag{3.3}$$

Here, t is the measurement time, E the energy of the channel and ε the detector efficiency. y_m and $E_{p,m}$ represent the intensity and energy of the mth peak of the nuclide n with an activity a_n. The shape function of gamma-ray peaks f_g is presented in Equation 3.1 and the baseline function f_b in Equation 3.2. In addition, the fitting region also contains K spectral shapes S_k scaled with multipliers D_k. The parameters a_n, C_0, C_1 and D_k can be selected to be either fixed of free. All free parameters inside the fitting region are fitted simultaneously.

The nuclide activity information can also be shared between the fitting regions in two ways. One possibility is to import a nuclide activity from an already fitted region. The imported activity can either be the initial starting value for the fitting process or, if no fitting is performed, the final activity used for the peak areas. Another possibility is to fit all parameters

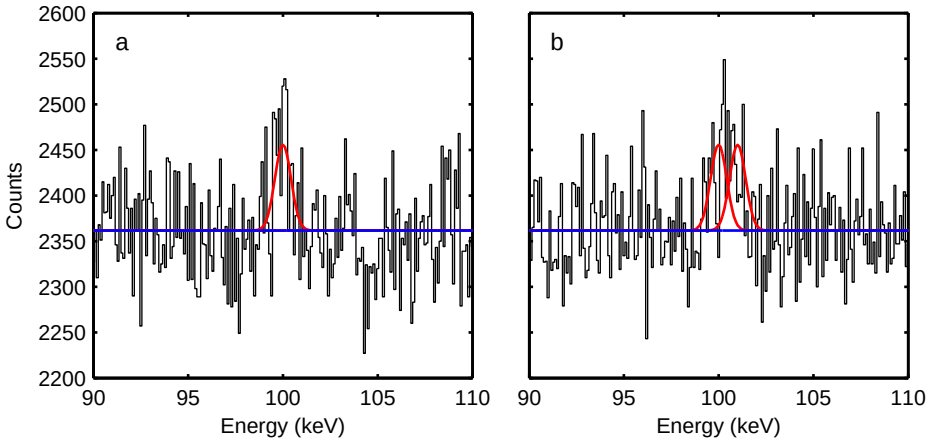

Figure 3.1. Part of a simulated gamma-ray spectrum containing one peak (a) or two overlapping peaks (b) with an area of 1000 counts. The red and blue lines show the ideal shape of the peak and the baseline.

in multiple regions of interest simultaneously. In this case, the peak areas between the fitting regions are also tied.

If the energy calibration is incorrect due to gain drift, the calibration can be fine tuned by fitting the peak locations. The fitted offset is constant for all peaks within the fitting region and the value of the maximum offset is limited. The allowed energy offset can also be defined relative to another fitting region.

3.2 Statistical properties

The statistical properties of AMUFI were reviewed by analysing a large number of simulated spectra. The spectra consisted of either one or two Gaussian peaks and a constant background (see Figure 3.1). The energy of the first peak was 100.0 keV and the full width at half maximum (FWHM) 1.0 keV. In the spectra containing two peaks, the peaks overlapped significantly. The second peak with same area and width as the first one resided at 101.0 keV. Each channel covered 0.1 keV in energy.

The areas of the simulated peaks ranged from 10 to 10 000 counts, and the baseline levels were selected to set the peak close to the limit of detection (see Table 3.1). The baseline level was solved from Equations 2.3 and 2.4 for P_α and P_β probabilities of 0.001. The value used for L_D was 85.9% of the nominal peak area, and it corresponds to an energy range of 1.25 times the peak FWHM. This range minimises the relative uncertainty of the signal in the analysis based on the total number of counts in a single energy region [42].

Table 3.1. Nominal peak areas and baseline levels used in the simulated spectra to test the statistical properties of AMUFI.

Peak are	Baseline level (1/keV)
10	0.030
50	37
100	190
1000	24000
10000	2400000

For each peak configuration, 1 000 simulated spectra were analysed with AMUFI. The energy of the fitting region was from 80 to 120 keV. For baseline, a linear model with two free parameters was used. The peak energies and energy calibration were considered to be well known.

The peak areas reported by AMUFI were unbiased and uncertainty estimates reliable as long as the areas of the simulated peaks stayed above 100 (see Figure 3.2). This also applied to spectra with overlapping peaks (see Figure 3.3). However, if the nominal number of counts per peak fell below 50, the reported peak-area uncertainties were slightly too small. For spectra consisting of peaks with only 10 counts residing on a baseline very close to zero, both the peak areas and their uncertainties were substantially underestimated.

3.3 Application to dating of a nuclear release

In May 2010, air-sampling stations in South Korea, Japan and the Russian Federation detected different unstable xenon isotopes and their progenies attached to aerosol particles. The origin of these fission products remains unclear. Other studies have suggested that a possible reason for these observations is a nuclear test performed in North Korea in May 2010 [43, 44, 45] . However, the lack of a seismic signal does not support this interpretation [46].

Of the isotope findings, the simultaneous detection of ^{140}Xe progenies ^{140}Ba and ^{140}La in the particulate samples collected in Okinawa, Japan, is especially interesting. Assuming a sudden release in the form of ^{140}Xe, the ratio of these nuclides reveals the timing of the release.

Analysis and results To verify the detection of ^{140}Ba and ^{140}La, AMUFI was applied to analyse all HPGe gamma-ray spectra collected and measured in Okinawa in 2010. The analysis is presented in detail in

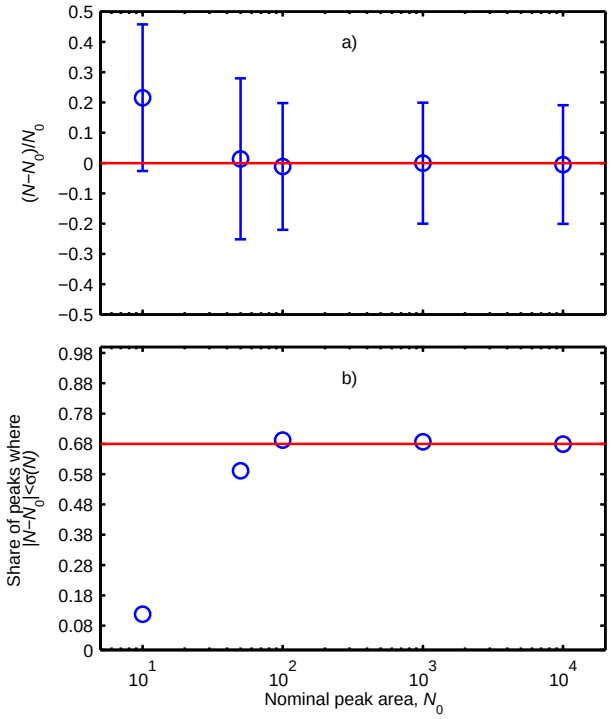

Figure 3.2. a) Mean and standard deviations of the fitted peak areas (N) relative to the nominal peak area (N_0). b) Proportion of fitted peak areas (N) within a standard uncertainty limit ($\sigma(N)$) from the nominal peak area (N_0). The data have been obtained from simulated spectra containing one peak.

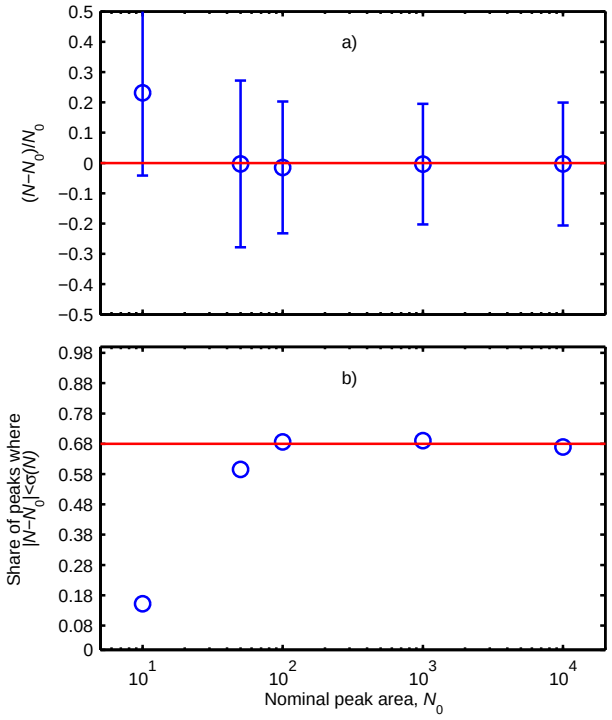

Figure 3.3. a) Mean and standard deviations of the fitted peak areas (N) relative to the nominal peak area (N_0). b) Proportion of fitted peak areas (N) within a standard uncertainty limit ($\sigma(N)$) from the nominal peak area (N_0). The data have been obtained from simulated spectra containing two overlapping peaks.

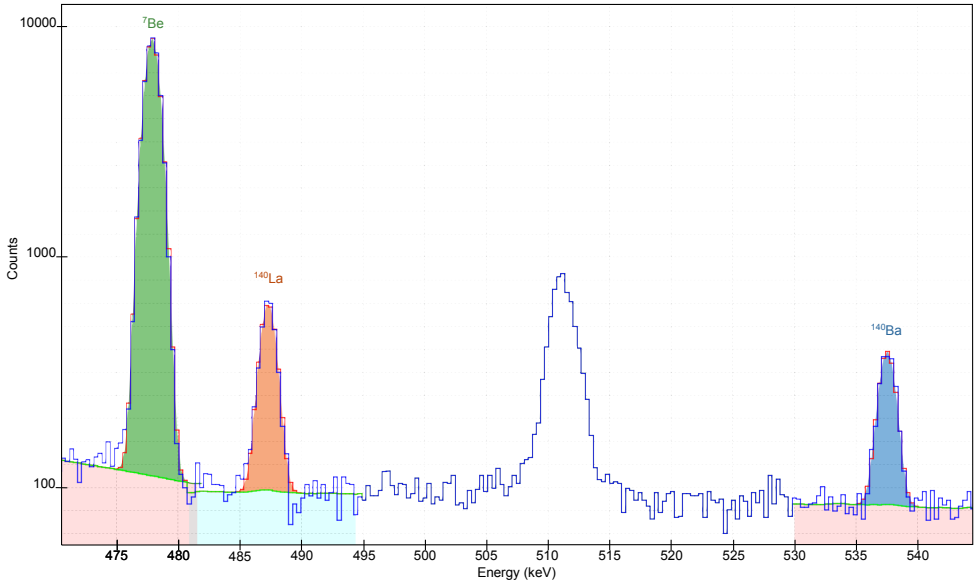

Figure 3.4. Gamma-ray spectrum containing clear ^{140}La and ^{140}Ba peaks analysed with AMUFI (acquisition time of 24 h). The highlighted areas below the peaks show the fitting regions. The natural ^{7}Be peak has also been fitted, whereas the 511 keV annihilation peak was not used in the analyses. The sample was collected in Okinawa on 15 May 2010. Adapted from Publication VI.

Publication VI of this thesis. Contrary to a previous interactive analysis of these spectra [43], the peak areas were now solved fully automatically. The automated analysis procedure eliminates the possible bias caused by the user in interactive analysis. This is especially important in the analysis of small peaks, where even a small adjustment of the baseline may have a large impact on the peak area.

For the analysis, the spectrum was divided into three fitting regions (see Figure 3.4). The 477.6 keV peak of ^{7}Be in the first region was used to obtain a good reference to compensate offsets of about 1 keV in the energy calibration during the year 2010. Two other fitted regions contained the 487.0 keV ^{140}La and 537.3 keV ^{140}Ba peaks. To take into account the peaks of naturally occurring radionuclides and other nonlinearities, the baseline shape used for ^{140}La and ^{140}Ba fitting regions was a smooth background spectrum scaled with a free multiplier. All regions were fitted simultaneously.

The detection of ^{140}Ba and ^{140}La in the successive samples collected between 15 and 21 of May 2010 was clear and cannot be explained with statistical variations (see Figure 3.5). Based on the analyses of the 2 h preliminary spectra of these samples, our best estimate for the release time was 12 May 16:00. Figure 3.6 presents the theoretical ^{140}La/^{140}Ba ratio fitted to the measured data. For dating, only spectra with sufficiently

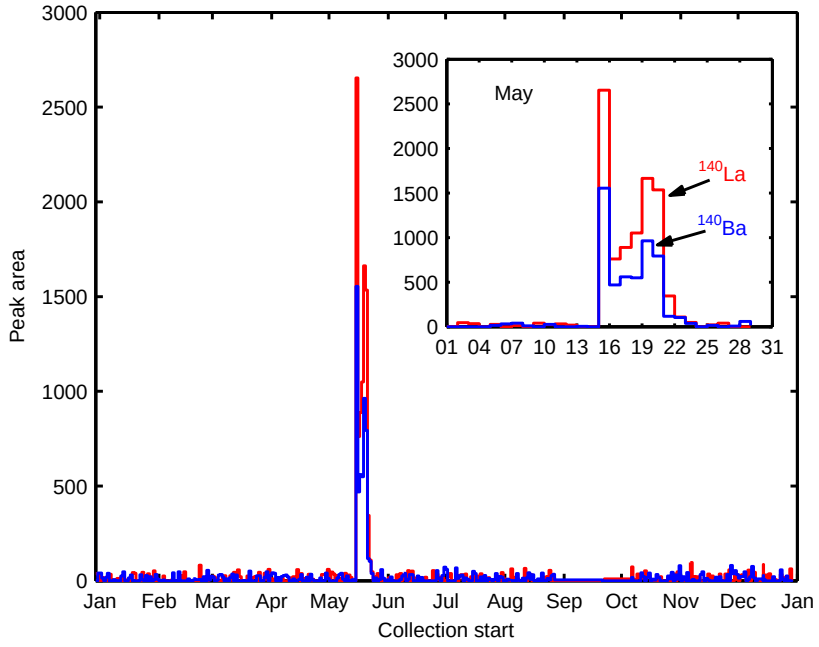

Figure 3.5. ^{140}La (487 keV) and ^{140}Ba (537 keV) peak areas in 24 h spectra collected in Okinawa in 2010. Adapted from Publication VI.

large peak areas were accepted. Taking the statistical uncertainty of the fitted peak areas into account and allowing a realistic 5% variation in the measurement setup parameters, the possible time interval of the release spread to 9 May 12:00–14 May 3:00. The dominant source of the measurement setup uncertainty was the coincidence correction factor for ^{140}La, which could not be determined precisely.

3.4 Conclusions

AMUFI is a powerful tool for the automated analysis of gamma-ray spectra with very different resolutions (NaI, $LaBr_3$, HPGe). In this thesis, the software program was exploited for the analysis of HPGe gamma-ray spectra acquired by the CTBTO International Monitoring Network (IMS). AMUFI and its simplified version, JMUFI, are also routinely used for analysing data from in-situ gamma-ray measurements with $LaBr_3$ and NaI detectors at STUK.

AMUFI is especially suited for the deconvolution of overlapping peaks. Reliable uncertainty estimates are obtained by taking into account the correlations between all fitted parameters. The capability to tie the peak areas together based on a nuclide library can further facilitate the multiplet analysis. Due to these two features, the code was capable of analysing complex $LaBr_3$ spectra containing multiple overlapping peaks

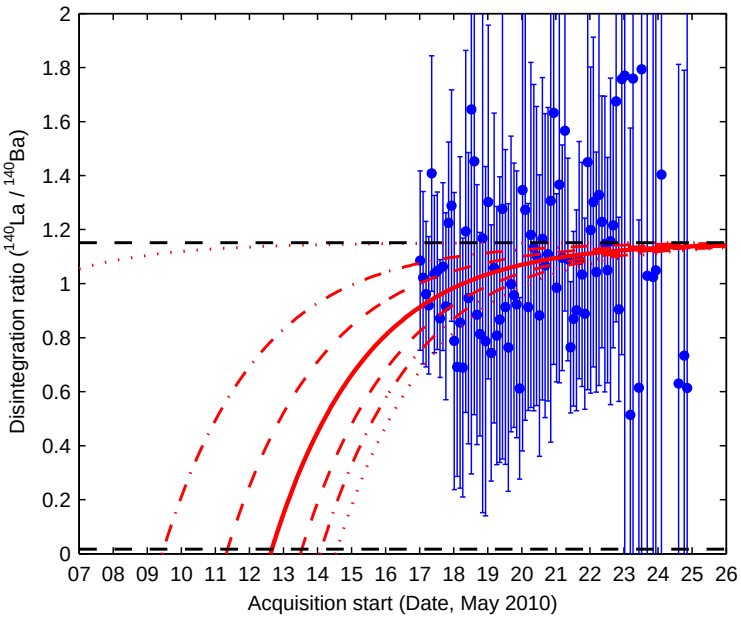

Figure 3.6. Modelled time behaviour of the ^{140}La/^{140}Ba disintegration ratio fitted to the measured data points from 2 h spectra. The dashed curves show the 95% confidence limits for measurement setup uncertainties (ΔC) of 0, $\pm$0.05 and $\pm$0.10. The horizontal dashed lines indicate the time-zero and equilibrium levels. The uncertainties of the data points refer to the peak area statistics alone. Adapted from Publication VI.

of various iodine and caesium isotopes during the Fukushima Dai-ichi accident.

A significant limitation in the current AMUFI version (2.8) is its incapability to resolve peaks with very low statistics. Based on the analysis of simulated spectra, both the peak areas and their uncertainties are significantly underestimated if most of the channels on the fitting region contain only one count or no counts at all. The problem arises from the fitting method that approximates the variation of the number of counts in each channel with the Gaussian distribution. In the future, the fitting routine should be optimised with a similar fine-tuning approach as the one applied for the analysis of alpha-particle spectra (see the next chapter).

4. Analysis of alpha-particle spectra

In radioanalytical laboratories, high-resolution alpha-particle spectrometry is a standard analysis method, which can be used to reveal small concentrations of alpha-particle-emitting radionuclides. Typically, the samples are first dissolved, and then the elements of interest are chemically separated and electrodeposited on a metal disc [47]. A high-resolution spectrum is obtained by measuring the sample with a semiconductor detector, such as Passivated Implanted Planar Silicon (PIPS), in a vacuum. These procedures minimize the number of overlapping peaks in the spectrum. Therefore, the activity and isotope analysis can often be based on a simple region-of-interest method. To determine the activity of the original sample, radioactive tracers are necessary to account for the chemical recovery of the radioelement in question.

The use of high-resolution alpha-particle spectrometry can be essentially extended with advanced spectrum analyses. Detailed deconvolution allows the analysis of spectra with overlapping peaks. Therefore, the spectrum may consist of multiple peaks from different radionuclides, and chemical separation of elements may not be required. The ideal geometry of the sample is also not as crucial, and the collected samples can sometimes even be measured as such or after minimum manipulation. Furthermore, if the sample quality is favourable, deconvolution makes it possible to distinguish between isotopes having alpha-particle energies very close to each other.

A number of computer codes with varying degrees of complexity exist for the analysis of alpha-particle spectra (see Reference [48] and references therein). Although commercial codes usually focus on stable and reliable operation, they may face difficulties in unfolding of the spectra with multiple overlapping peaks. In the IAEA Coordinated Research Programme, a set of commercial programs was compared [49].

The final conclusion of the IAEA report was that “it is clear from the results that there is room for improvement ...”. In addition, “all programs exhibit lack of statistical control, especially where the deconvolution of multiplets or analysis of spectra with very good statistics are concerned: uncertainties in reported peak areas are underestimated in all cases.” The present thesis shows that reliable uncertainty estimates can be obtained with detailed peak-shape modelling and covariance calculus of unknown parameters.

One challenging problem for any alpha-particle spectrum analysis program is the unfolding of the ^{239}Pu-^{240}Pu multiplet [50]. These isotopes of Pu are of special concern in nuclear safeguards and arms control, since their ratio distinguishes ordinary reactor plutonium from weapons-grade material. The energies of the dominant alpha-particle emissions of ^{239}Pu and ^{240}Pu differ by only 12 keV (see Table 1.1), which is of the same order of magnitude or less than the typical energy resolution of a semiconductor alpha-particle detector. Vajda and Kim [51] even stated that “commercially available spectrometers and spectrum evaluation software are not adequate for the measurements of ^{239}Pu and ^{240}Pu independently.“ Due to its importance, the determination of this ratio has been investigated in this thesis and also in a number of other scientific papers (see for example References [52, 53, 54, 55, 56, 57]).

In addition to the above-mentioned isotopes, there are other important pairs of radionuclides, such as ^{238}Pu and ^{241}Am, which are difficult to identify unambiguously using alpha-particle spectrometry because of limited energy resolution [58]. The unfolding procedure has also been investigated for isotopes, such as ^{243}Cm and ^{244}Cm [54] and ^{241}Am and ^{243}Am [59] , where the overlap of peaks from different nuclides is not as marked as for ^{239}Pu and ^{240}Pu.

4.1 ADAM analysis software

To respond to the call for a tool for unfolding complex alpha-particle spectra, an analysis program called ADAM[1] (Advanced Deconvolution of Alpha Multiplets) was developed. The software is designed for routine

[1]ADAM was coded for STUK by Andreas Pelikan, Dienstleitungen in der automatischen Datenverarbeitung und Informationstechnik, Austria. Other people contributing to the development of the software are Harri Toivonen (project management and architecture), Sakari Ihantola (algorithms and testing) and Roy Pöllänen (usability and testing).

analysis of spectra obtained from different sample types such as air filters, swipe samples and radiochemically processed sources measured in a vacuum with high-resolution detectors. Effective spectrum handling is enabled with versatile analysis tools, an extensive nuclide library, an intuitive graphical user interface and a direct link to an open-source database (LINSSI [40]) with sophisticated browsing tools. In the development of ADAM, the key design principle was to create a code that has high statistical control in the deconvolution of multiplets and which produces realistic uncertainties for reported activities.

Peak shape The standard peak-shape model used in ADAM and several other analysis programs for alpha-particle spectra was suggested by Bortels and Collaers [60]. In this model, the peak shape is a convolution of a Gaussian function and a sum of one-sided exponentials. Typically, one exponential can adequately describe peaks with low statistics, whereas up to three tail functions may be required for peaks with high statistics [61, 56].

Mathematically, the shape of a fitted peak can be expressed as

$$f_\alpha(E) = \int_{-\infty}^{\infty} f_e(E') f_g(E - E') \mathrm{d}E', \tag{4.1}$$

where

$$f_e(E') = \begin{cases} \sum_{n=1}^{N} \underbrace{c_n \exp\left(\nu_n (E' - E_p)\right)}_{e_n} & \text{if } E' \leq E_p \\ 0 & \text{if } E' > E_p \end{cases} \tag{4.2}$$

and

$$f_g(E - E') = \frac{1}{\sqrt{2\pi\sigma^2}} \exp\left(-\frac{(E - E')^2}{2\sigma^2}\right). \tag{4.3}$$

Here, E denotes the energy of the channel and E_p the nominal energy of the peak. E' is the variable of integration. The shape parameter ν_n describes the slope of the nth exponential function e_n. The smaller the value of the shape parameter, the slower the tail decreases. c_n is a normalisation constant. The only shape parameter of the Gaussian function, σ, is proportional to the FWHM (Full width at half maximum).

Unfortunately, the parametrised model cannot adequately describe the peaks affected by coincidence summing [62]. Since an alpha decay is often followed by X-ray, low-energy gamma-ray, conversion electron or Auger electron emissions, the true coincidences are common in close-geometry alpha-particle measurements with high efficiency [63]. The result of the coincidences is that the alpha-particle counts originating from the excited

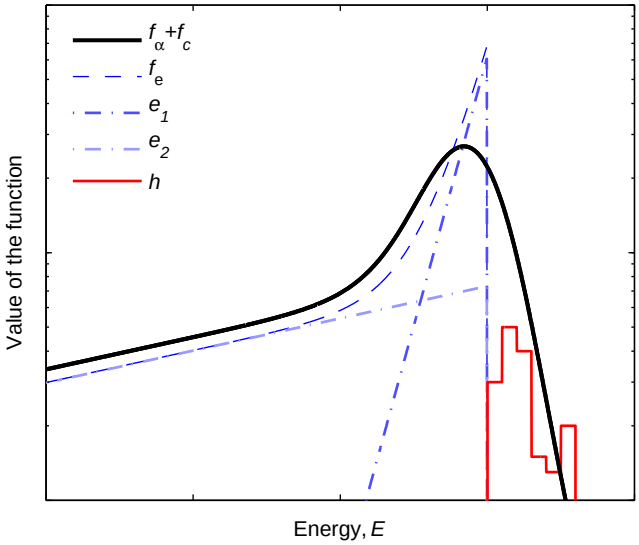

Figure 4.1. An example of the total peak shape model ($f_\alpha + f_c$) consisting of two exponentials ($f_e = e_1 + e_2$) and a coincidence spectrum (h) on a logarithmic scale.

states may appear at higher energies, which considerably affects the peak shapes. The coincidence component is individual for each alpha-particle transition.

One unique feature of ADAM is that it can take these coincidences into account (see Figure 4.1). The coincidences are modelled by importing the energy spectrum h of the electrons and photons in coincidence with an alpha particle. The coincidence shape f_c is a convolution of this spectrum h and alpha-particle peak shape f_α:

$$f_c(E) = \int_{-\infty}^{\infty} h(E') f_\alpha(E - E') \mathrm{d}E'. \tag{4.4}$$

ADAM imports the energy spectra from the Aasi Monte Carlo code [64].

Calibrations In contrast to gamma-ray spectrometry, the peak shapes in alpha-particle spectrometry strongly depend on the sample characteristics and measurement geometry. In vacuum, thicker samples and shorter source-to-detector distances produce broader peak shapes and heavier tailing due to the energy absorption of alpha-particles. Therefore, a fixed shape calibration cannot be used; instead, the calibration must be selected according to the sample type. Since small differences in the sample geometry are common even within samples of the same type, the shape parameters are typically kept free whenever feasible. Keeping the shape parameters fixed is only reasonable in the analysis of low-statistics spectra from a well-known measurement setup where the shape parameters have been

accurately determined based on a previous measurement with high statistics. Fortunately, the alpha-particle peak shapes do not markedly depend on the energy of the line. Therefore, the same shape can be typically used for all lines. Only if the materials are inhomogeneously distributed in the sample, it may be required to use different shapes for different nuclides.

The efficiency and energy calibration functions needed in alpha-particle spectrometry are commonly simple. For samples thin enough not to fully absorb the alpha particles, the efficiency calibration is a constant depending only on the geometrical detection efficiency. For energy calibrations, ADAM uses polynomials up to third order. In a typical energy range of interest, the output of PIPS detectors is linear with respect to the energy of the alpha particle. The advantages of second- or third-order energy calibration functions are apparent only in applications with high counting statistics [65]. However, the energy calibration also depends somewhat on the sample and measurement geometries. Therefore, it is often required to fine-tune the calibration by fitting the energy calibration parameters together with the peak-shape parameters during spectrum analyses.

Fitting One challenge in the analysis of alpha-particle spectra is the large number of free parameters to be fitted. As discussed previously, it may be necessary to fit 2 to 6 shape parameters together with at least one energy calibration parameter. In addition, each nuclide present may have several peaks. Since the calibration parameters are competing and peaks often overlapping, it is preferable to fit all parameters simultaneously.

In ADAM, the nuclear library data is maximally utilised to reduce the number of free parameters. Based on the library data, both the peak energies and relative areas are kept fixed during fitting. Such constrained fitting provides the tool to unfold complex multiplets, increases the accuracy of the activity ratio calculus and speeds up the fitting process [66].

The fitting and uncertainty estimation is based on the methods described in Section 2.2. The fitted function is

$$f(E) = \sum_{i=1}^{I} A_i \sum_{j=1}^{J_i} y_j (f_\alpha(E, E_{p,j}) + f_c(E, E_{p,j}), \tag{4.5}$$

where A_i is the total area of nuclide i emitting alpha particles at J_i different energies. $E_{p,j}$ and y_j are the energy and yield of the jth alpha line. The alpha-particle peak shape f_α is presented in Equation 4.1 and the coincidence shape f_c in Equation 4.4. Since the alpha-particle spectra

are generally almost free from external background, the total shape only consist of alpha-particle peaks.

Strictly speaking, the fitting method relying on the least-squares method is valid only if the number of counts in each channel is large enough to be approximated with a Gaussian distribution. However, the low-background alpha-particle spectra may contain multiple channels with very few or even zero counts. To overcome this problem, the elements of the weight matrix $\boldsymbol{W}$ (see Equation 2.18) in ADAM are calculated from values of the fitted function in the previous iteration:

$$\sigma_n = \sqrt{f(E_n, \beta, c) + 1}. \tag{4.6}$$

The use of a fitted number of counts instead of measured counts rejects the biasing of the fit for low-statistics spectra [67]. The factor one needs to be added to reduce the weight of the channels with only a few counts, since those channels can hardly be approximated with a Gaussian distribution.

Sometimes, the peak shapes cannot adequately describe the measured spectrum, which reduces the reliability of the results. Such a case may occur, for example, if the coincidence phenomena are not taken correctly into account. In the current ADAM version (2.9.4), the possible overdispersion is compensated by multiplying the uncertainties calculated with Equation 2.23 by a factor χ_r^2:

$$\chi_r^2 = \frac{1}{N} \sum_{n=1}^{N} \left(\frac{f_n - y_n}{\max\left(\sqrt{f_n}, 1\right)} \right)^2. \tag{4.7}$$

For a perfect model, $\chi_r^2 \approx 1$. The worse the fit, the larger the χ_r^2. A disadvantage of this method is that it extends the uncertainty limits of all fitted parameters with the same factor. For example, for a spectrum containing two separate peaks, the uncertainties of both peaks are equally extended, even though the fit of only one peak is faulty. Therefore, this method cannot be justified as a general approach.

4.2 Statistical properties

The statistical properties of ADAM were studied with three series of experiments presented in Publication II. First, the ADAM software was tested by using simulated spectra containing one peak. Peak areas from 10 to 10 000 were used, and 10 000 spectra were analysed corresponding to each area. Second, to test multiplet fitting, the same set of analyses was performed by using simulated spectra containing two overlapping peaks.

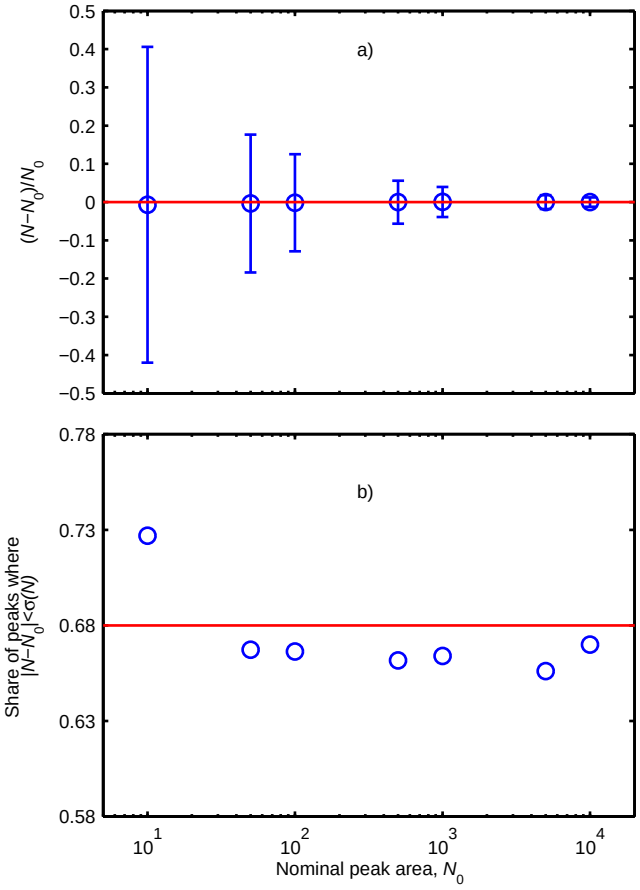

Figure 4.2. a) Mean and standard deviations of the fitted peak areas (N) relative to the nominal peak area (N_0). b) Proportion of fitted peak areas (N) within a standard uncertainty limit ($\sigma(N)$) from the nominal peak area (N_0). The data have been obtained from simulated spectra consisting of two peaks with known shape parameters. Adapted from Publication II.

Third, similar analyses were also carried out with real ^{148}Gd spectra. All analyses were repeated both by assuming the peak shape parameters to be known and unknown.

The peak areas and their uncertainty estimates given by ADAM were statistically correct (see Figure 4.2). This applied for all peaks, regardless of the peak area. The peaks can be either individual or multiplets, and the peak shapes can be known or extracted from the spectrum. The results obtained from analysing the simulated spectra were consistent with those from the measured spectra. The relative variance of the areas continuously decreased as the peak areas increased, making the estimate more precise. The variance of the fitted peaks was close to the minimum variance set by the Poisson statistics, proving the efficiency of the method. The differences in variance between the cases where the peak shapes were free or fixed were small. Thus, external shape calibration is often not

required, but the calibration can be well be extracted from the measured spectrum itself.

4.3 Application to plutonium analysis

To further validate the code, the ADAM software was applied to analysis of alpha-particle spectra from radiochemically processed sources containing ^{238}Pu, ^{242}Pu and varying amounts of ^{239}Pu and ^{240}Pu. The analyses are described extensively in Publication III. The focus was to determine the activity ratios of ^{239}Pu and ^{240}Pu. Due to the small energy difference between the ^{239}Pu and ^{240}Pu lines, the accuracy of this ratio is sensitive to any shortcomings of the software and reveals the deficiencies of the spectrum analysis procedure. The sources were analysed blind, i.e. the isotopic ratios were not known beforehand. The peak shape and energy calibration parameters were taken from each of the measured spectra.

The deconvolution of the alpha-particle spectra with different isotopic ratios was successful (see Figure 4.3). In spectrum unfolding, three exponential functions were necessary to explain the peak tailing in high statistics spectra. In addition, a second-order polynomial for the energy calibration gave a better fit compared to the linear channel-energy response, although the difference was small. Moreover, coincidences between alpha particles and low-energy photons/electrons simulated with Aasi Monte Carlo code had to be accounted for to obtain best possible results in the fitting.

The ^{239}Pu/^{240}Pu isotopic ratios calculated from the alpha-particle spectra coincided well with the reference values (see Table 4.1). Since there is a strong overlap between the peak families of ^{239}Pu and ^{240}Pu, the correlation between the peak areas cannot be neglected in the uncertainty estimation of the peak area ratio with Equation 2.32. The minimum value in Equation 2.29 was used for covariance terms because the correlation coefficients of ^{239}Pu and ^{240}Pu peak areas were always very close to -1 (perfect negative correlation). By analysing spectra with different counting statistics, the standard uncertainty of the ^{239}Pu/^{240}Pu activity ratio was determined to be less than 10% if the total number of counts in the ^{239,240}Pu peak family was larger than approximately 1000.

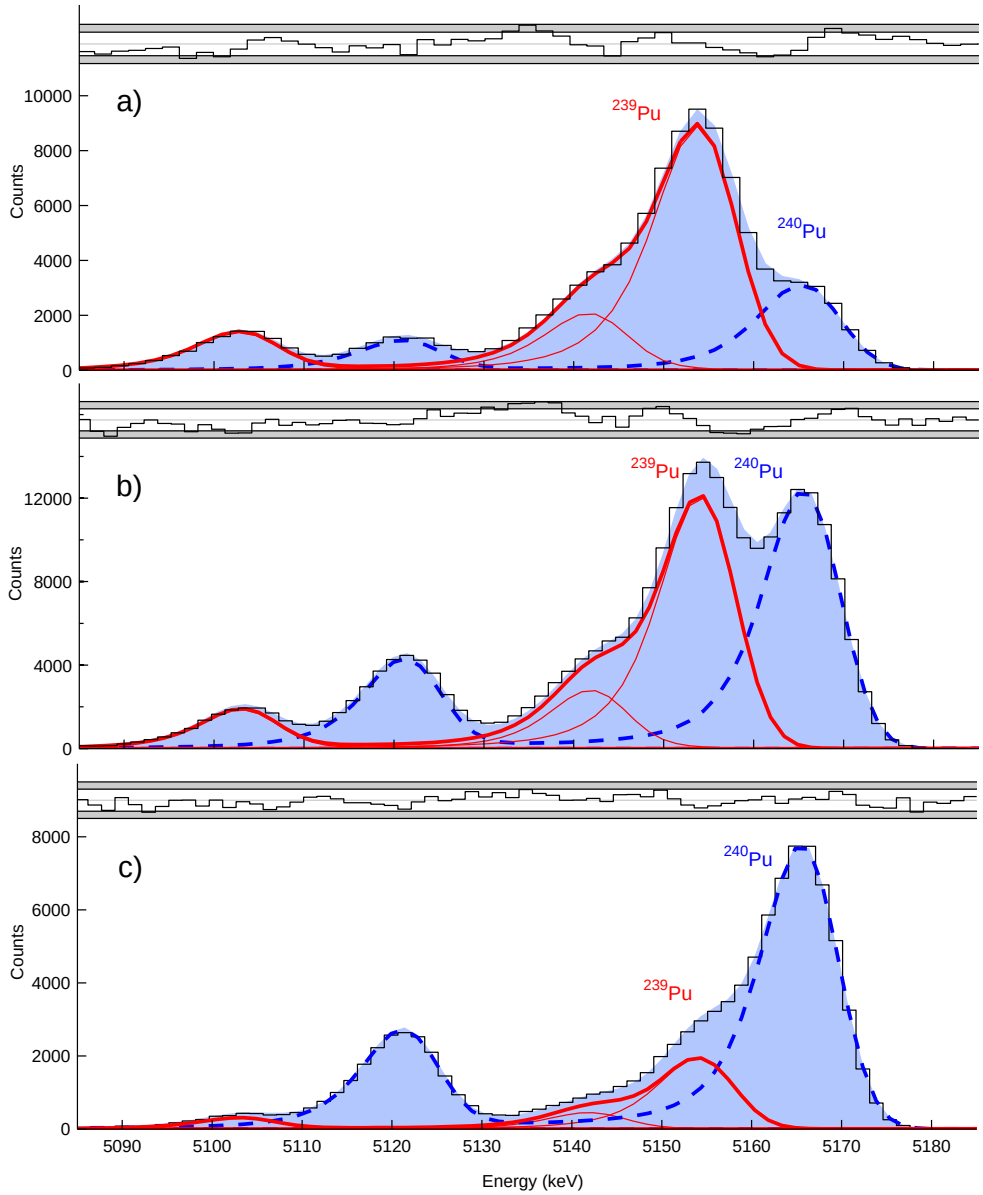

Figure 4.3. Alpha-particle energy spectra from three sources containing ^{239}Pu and ^{240}Pu isotopes in different ratios fitted with ADAM. Individual peaks and their sum are shown as lines whereas shaded areas represent total fits. The residual with the limits of 3 and 5 standard deviations (grey areas) is presented at the top of each figure. Adapted from Publication III.

Table 4.1. ^{239}Pu/^{240}Pu activity ratios with expanded uncertainties (coverage factor k=2) from measurements at source-to-detector distances (SDD) of 9 mm and 48.5 mm compared to the NIST reference values. Adapted from Publication III.

SDD 9 mm	SDD 48.5 mm	NIST reference value
0.256 ± 0.009	0.258 ± 0.008	0.248 ± 0.003
1.00 ± 0.02	1.03 ± 0.05	1.00 ± 0.01
2.93 ± 0.09	2.9 ± 0.2	3.01 ± 0.03
2.88 ± 0.09	2.9 ± 0.2	2.91 ± 0.03
1.01 ± 0.03	1.00 ± 0.03	0.98 ± 0.01
0.408 ± 0.009	0.42 ± 0.03	0.398 ± 0.004

4.4 Conclusions

The alpha-particle spectrum analysis program ADAM is well suited for the deconvolution of spectra consisting of overlapping peaks. Reliable uncertainty estimates for the peak areas are obtained by taking into account the correlations between all fitted parameters. Another crucial feature is the detailed peak-shape model, which is capable of resolving the influence of the photons and electrons in coincidence with alpha particles.

Due to these unique features, even the ^{239}Pu/^{240}Pu isotopic ratio, which is especially important for nuclear safeguards, can be reliably determined with high-resolution alpha-particle spectrometry. The successful analysis of the ^{239,240}Pu spectra is also an excellent proof of the analysis capabilities of ADAM. For other pairs of nuclides with a larger difference in the energy of the emitted alpha particles, the tolerance of overlapping peaks makes the high quality of the sample less critical and may remove the need for the chemical separation of the elements.

The peak areas and their uncertainty estimates given by ADAM are statistically correct even for peaks consisting of only 10 counts. The result is somewhat surprising, considering that the fitting procedure in ADAM relies on the Gaussian statistics. The high accuracy for spectra with small peaks was obtained by optimising the fitting to reduce the weight of the channels with a low number of counts. The ability to analyse low-statistic spectra is essential in several applications, such as environmental monitoring and nuclear forensics.

5. Alpha-gamma coincidence

In coincidence measurements, the radionuclide is characterised by signals simultaneously detected with multiple detectors. The technique allows more precise focusing of the measurement on certain types of events, which reduces the background that disturbs the detection of small signals. In coincidence measurement mode, only those events that occur within a small time window are accepted. In anti-coincidence mode, the events simultaneously detected in multiple detectors are considered as background and removed from the data used for the analysis.

Coincidence techniques were widely used for the characterisation of environmental samples in the 1960s because of the lack of high-resolution spectrometers able to provide the required selectivity. The need to detect lower and lower activities has brought renewed interest in these techniques. Nowadays, several analytical laboratories are utilising or planning to utilise the anticoincidence mode for background suppression in gamma-ray spectrometry [68, 69, 70, 71, 72]. An annulus of low-resolution gamma-ray detectors (typically NaI or BGO) around a high-purity germanium detector is used to identify scattered photons causing the Compton continuum in the recorded spectrum (see Reference [73] and references therein). To remove events caused by cosmic muons, the detector lead shields are covered with large plastic scintillators (see Reference [69] and references therein).

The coincidence mode also plays a significant role in specific applications. For example, antineutrino detectors planned for reactor monitoring are based on the detection of positrons in coincidence with neutrons [74]. The very low background rate achieved allows the detection of antineutrinos via a rare inverse beta decay reaction. At the CTBTO noble gas analysis stations, a high sensitivity and selectivity for different xenon isotopes is achieved with electron-X-ray coincidence using a 4π beta detec-

tor [75, 76]. The gamma-gamma coincidence approach has been shown to be feasible for uranium analysis [77] and for the detection of ^{22}Na from air filters [78, 79]. Alpha-gamma -coincidence is not yet used widely. The technique has mainly been utilised for the characterisation of nuclide properties in basic research [80]. Only the IAEA Safeguards Analytical Laboratory has studied this approach for transuranium detection [81].

The flexible use of coincidence techniques has greatly benefited from advancements in digital signal processing and list-mode data acquisition. In list-mode data acquisition, the time and amplitude of each event is recorded. When data from multiple detectors with synchronised clocks are combined, multiple singles, coincidence and anticoincidence spectra can be generated. Thus, the coincidence parameters do not need to be selected during the measurement phase but can be adjusted during analysis. The fast digital electronics allow the use of very short coincidence time windows ($\tau < 10$ ns), only limited by the detector properties (variety in charge collection time typically over 100 ns for HPGe).

5.1 Methods for activity determination

A textbook example of the coincidence techniques is the activity determination of a source by using the gamma-gamma or beta-gamma approach [82]. With a coincidence technique, the detection efficiencies can be resolved without any knowledge of the source activity or measurement geometry. Therefore, the source activity can be precisely determined without a separate calibration measurement.

The basis of the activity determination with the coincidence method is that the coincidence probability (ε_{12}) is a product of individual detection probabilities (ε_1 and ε_2):

$$\varepsilon_{12} = \varepsilon_1 \varepsilon_2. \tag{5.1}$$

Two criteria commonly overlooked need to be fulfilled to use this method. First, the emission directions of the particles or photons cannot be correlated. Second, the detection efficiency for either type of radiation must be constant over the source. The first criterion is violated if annihilation photons are used for the activity determination of a source in a gamma-gamma coincidence setup. The second criterion limits the size of the source.

Here we concentrate on efficiency and activity determination in alpha-gamma coincidence measurements. Techniques are first described for

radionuclides observed both in singles and coincidence spectra. Then, the results are extended for nuclides only detectable in coincidence spectra. The measurement live times of the spectra are considered to be equal.

Alpha-particle detection efficiency For a nuclide detected both in the alpha-gated and singles gamma-ray spectra, the alpha-particle detection efficiency can be calculated as follows:

$$\varepsilon_\alpha = \frac{\varepsilon_{\alpha\gamma}}{\varepsilon_\gamma} = \frac{A_{\alpha\gamma}/(ay_\gamma t)}{A_\gamma/(ay_\gamma t)} = \frac{A_{\alpha\gamma}}{A_\gamma}. \tag{5.2}$$

Here, $A_{\alpha\gamma}$ is the peak area in the alpha-gated gamma-ray spectrum and A_γ the area of the same peak in the singles gamma-ray spectrum. The activity of the sample a, measurement time t and the yield of the observed gamma-ray transition y_γ cancel out.

The alpha-particle detection efficiency obtained depends on the energy of the alpha particle, energy limits of the selected alpha gate and measurement geometry. If the selected gate does not reduce the number of recorded alpha particles, the efficiency is constant regardless of the alpha-particle energy.

Gamma-ray detection efficiency For a nuclide reliably determined both in the alpha-gated gamma-ray and singles alpha-particle spectra, the gamma-ray detection efficiency can be calculated as follows:

$$\varepsilon_\gamma = \frac{\varepsilon_{\alpha\gamma}}{\varepsilon_\alpha} = \frac{A_{\alpha\gamma}/(ay_\gamma t)}{A_\alpha/(ay_\alpha t)} = \frac{A_{\alpha\gamma}y_\alpha}{A_\alpha y_\gamma}. \tag{5.3}$$

The spectra used to calculate the gamma-ray peak area $A_{\alpha\gamma}$ must be generated with the same energy limits for the alpha-particle gate as were used to calculate the area A_α in the alpha-particle spectrum. Again, a and t cancel out.

For complex alpha-particle spectra, the spectrum analysis can be simplified by first analysing a gamma-gated alpha-particle spectrum consisting only of a single nuclide. The peak shape determined from the gated alpha-particle spectrum is then used to deconvolute the singles alpha-particle spectrum.

Activity of a nuclide visible in singles and gated spectra Determining the activity of a nuclide visible in the singles gamma-ray spectrum, singles alpha-particle spectrum and alpha-gated gamma-ray spectrum is straightforward. The activity is calculated by combining the gamma-ray efficiency from Equation 5.3 with the peak area in the singles gamma-ray spectrum:

$$a = \frac{A_\gamma}{\varepsilon_\gamma y_\gamma t} = \frac{A_\gamma A_\alpha}{A_{\alpha\gamma} t y_\alpha}. \tag{5.4}$$

Activity of a nuclide only visible in gated spectra The activity of any nuclide visible in alpha-gated gamma-ray spectrum can be calculated with the equation

$$a = \frac{A_{\alpha\gamma}}{\varepsilon_\alpha \varepsilon_\gamma y_\gamma t}. \tag{5.5}$$

For nuclides only visible in gated spectra, determining the efficiencies ε_α and ε_γ is more complex. Now, Equations 5.3 and 5.2 cannot be directly used for efficiency calculus, since the areas A_γ and A_α are not known.

If the sample contains some nuclides visible in both singles and gated spectra, these nuclides can be used to increase the accuracy of the activity determination for nuclides that are only visible in gated spectra. The reference nuclides visible in both spectra fix the absolute level of the efficiency curves. Therefore, only the shapes of the efficiency curves are required to extract the efficiency for the nuclide of interest:

$$\varepsilon_\alpha(E) = \varepsilon_\alpha(E_{\text{ref}})[1 - \Delta\varepsilon_\alpha] \tag{5.6}$$

$$\varepsilon_\gamma(E) = \varepsilon_\gamma(E_{\text{ref}})[1 - \Delta\varepsilon_\gamma]. \tag{5.7}$$

Here, $\Delta\varepsilon_\alpha$ and $\Delta\varepsilon_\gamma$ are the efficiency differences between the reference nuclide and the nuclide of interest. This approach reduces uncertainties related to the measurement geometry and acquisition electronics. The method is especially accurate if the energy difference between the nuclides is small. The shapes of the efficiency curves required to determine $\Delta\varepsilon_\alpha$ and $\Delta\varepsilon_\gamma$ can be easily obtained from Monte Carlo simulations, since the absolute efficiencies are not required.

5.2 PANDA testbed for coincidence studies

The PANDA (Particles and Non-Destructive Analysis) testbed designed and built at the STUK is a platform for studying novel detectors and ideas. Measurement position 1 in PANDA is dedicated to examining the capabilities of alpha-gamma coincidence technique. It hosts a broad energy HPGe detector for the detection of gamma and X-rays and a double-sided silicon strip detector (DSSSD) for alpha particles. The detectors are mounted facing each other in a vacuum, and the samples are measured between them. A typical source-to-detector distance is in the range of 2-5 mm. The DSSSD used is a position-sensitive detector having 1024 pixels with a size of 2×2 mm^2. The grid consists of 32

front strips and 32 back strips. Each strip is 2 mm wide and 64 mm long, making the active area of the detector 64×64 mm^2. A detailed description of PANDA hardware is presented in References [83, 84].

To allow flexible analysis, data from both detectors are recorded in list mode. The time-stamped events together with supporting metadata are uploaded into a LINSSI database extended with tables for list-mode data. The coincidence resolving time of the events is 3 μs. The spectra for the analysis are generated from the events with a specific software program, which allows coincidence parameters to be freely selected. The software also includes algorithms to combine different measurements, to match the gain of different strips of the DSSSD and to locate particles based on the DSSSD hitmap [85].

5.3 Application to characterisation of a nuclear bomb particle

The alpha-gamma coincidence analysis conducted for a nuclear bomb particle is described in detail in Publication I. The particle was collected in Thule, Greenland, in 1997 from the site where a US bomber carrying thermonuclear weapons crashed in 1968. Several authors have investigated the characteristics of individual particles from this nuclear bomb material, identified from sea sediment samples [86, 87, 88]. The characteristics of the particle used here have previously been studied by Pöllänen et al. [88] with scanning electron microscopy, alpha-particle spectrometry and gamma-ray spectrometry. The shape of the porous particle resembles an oval with a maximum length of 28 μm. The particle was measured in PANDA measurement position 1 for 20.8 d.

Figure 5.1a shows the ordinary singles gamma-ray spectrum and Figure 5.2a the ordinary singles alpha-particle spectrum of the sample. The alpha-particle spectrum was created by summing the spectra from the pixels closest to the particle. ^{241}Am is the only isotope in the sample that can be identified based on the singles spectra. The presence of plutonium is revealed by the X-rays visible at energies between 12 and 20 keV in the gamma-ray spectrum. The broad peak at around 5.5 MeV in the alpha-particle spectrum indicates either ^{239}Pu or ^{240}Pu. These two plutonium isotopes cannot be distinguished from each other. The attenuation in the non-ideal sample blends their alpha-particle emissions, which are very close to each other in energy (see Table 1.1). The X-rays are

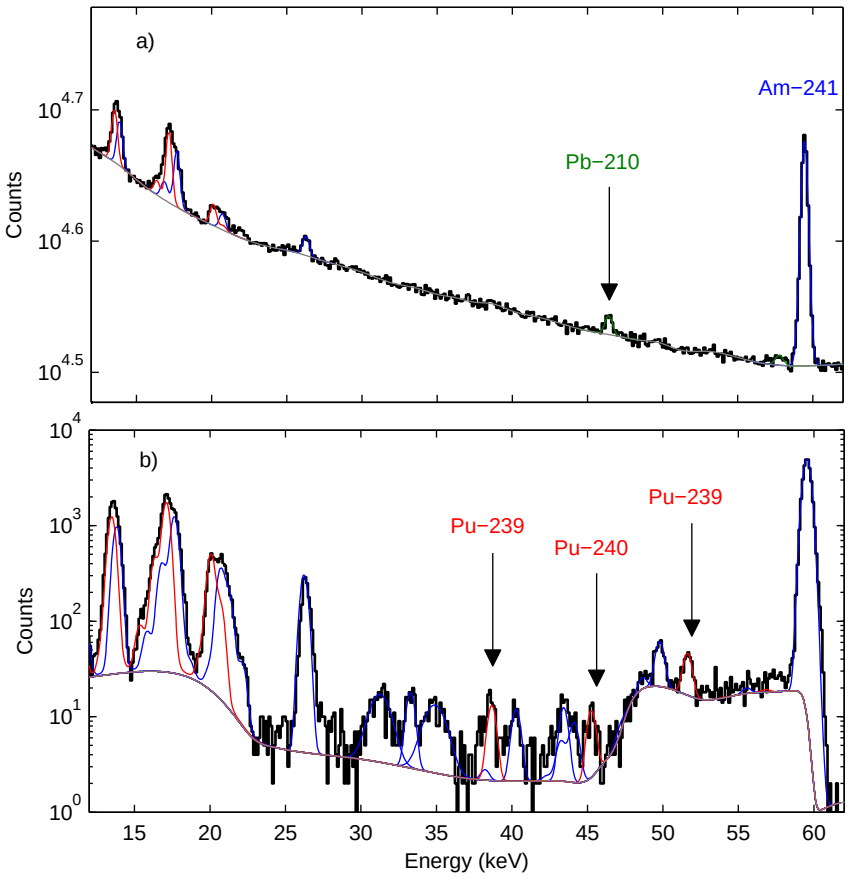

Figure 5.1. Singles (a) and alpha-gated (b) gamma-ray spectrum of the Thule nuclear bomb particle analysed with Aatami [36]. Adapted from Publication I.

not isotope specific, and the gamma rays of ^{239}Pu and ^{240}Pu are masked by the large background in the singles gamma-ray spectrum.

Figure 5.1b presents the alpha-gated gamma-ray spectrum, which is the most informative spectrum from the measured data. To generate the spectrum, gamma rays in coincidence with alpha particles having energies above 0.5 MeV were accepted. The alpha gate practically fully removed the counts not caused by the source itself, i.e. the effect of random coincidences is negligible. Due to the much reduced background, many new gamma-ray peaks are visible. ^{239}Pu can best be identified based on the 51.6 keV peak and ^{240}Pu based on the 45.2 keV peak. The presence of ^{235}U is clear based on the 185.7 keV peak (energy region not shown). The ^{241}Am identification from the alpha-particle spectrum can be verified by creating an alpha-particle spectrum gated with 59.5 keV gamma rays (see Figure 5.2b).

To estimate the relative plutonium isotope ratio based on the alpha-gated gamma-ray spectrum, the alpha-particle and gamma-ray efficiencies of the detectors are not required. Since the alpha-particle energies of

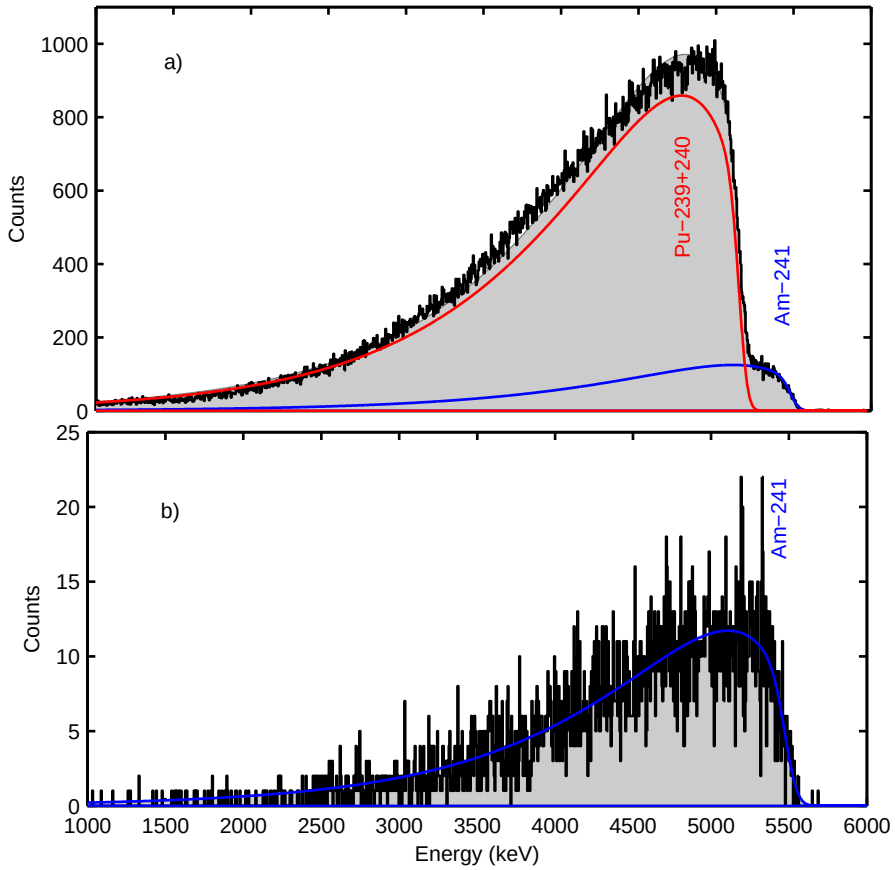

Figure 5.2. Singles (a) and 59.5 keV gamma-gated (b) alpha-particle spectrum of the Thule nuclear bomb particle analysed with ADAM. Adapted from Publication I.

^{239}Pu and ^{240}Pu are very close to each other, the alpha-particle efficiency is basically the same for both isotopes and they are therefore cancelled out from Equation 5.5 in the ratio calculus. It is also justified to use an identical detection efficiency for 51.6 keV (^{239}Pu) and 45.2 keV (^{240}Pu) gamma rays due to the flat efficiency curve of the germanium detector in this energy domain. In the present case, this simple approach gave a value of 0.950 $\pm$ 0.010 for the ^{239}Pu/(^{239}Pu+^{240}Pu) atom ratio. Notice that the uncertainty of the atom ratio is smaller than the nuclide activity uncertainties in Table 5.1, since the uncertainties related to the efficiency curve are not included.

The presence of ^{241}Am was utilised to accurately evaluate the absolute activities of the plutonium and uranium isotopes only visible in gated spectra. Since the ^{241}Am peak area can be determined from the singles gamma-ray spectrum, alpha-gated gamma-ray spectrum and singles alpha-particle spectrum, the ^{241}Am activity was calculated simply based on these areas with Equation 5.4. Likewise, Equations 5.2 and 5.3 were used to derive the efficiencies for ^{241}Am alpha particles and gamma

Table 5.1. Nuclide activities of the Thule nuclear bomb particle determined with alpha-gamma coincidence approach. The uncertainty values refer to the combined standard uncertainty. Adapted from Publication I.

Nuclide	Energy (keV)	Peak area	Activity (Bq)	Uncertainty (%)
^{241}Am	59.54	82783	0.42	7
^{239}Pu	51.62	179.4	3.4	15
^{240}Pu	45.24	56.1	0.66	19
^{235}U	185.71	14.7	0.00022	39

rays. To calculate the gamma-ray and alpha-particle efficiencies for the plutonium and uranium isotopes, the ^{241}Am efficiencies were used as the reference values ($\varepsilon(E_{\mathrm{ref}})$) in Equations 5.6 and 5.7. $\Delta\varepsilon_\alpha$ and $\Delta\varepsilon_\beta$ for each line were determined from simulated efficiency curves. The activities of the nuclides in the sample are presented in Table 5.1. The relative activities agree with the results previously obtained for similar particles collected in Thule.

The alpha-gamma coincidence technique reduced the MDA significantly compared to a singles gamma-ray measurement. Under these experimental conditions, the MDA of alpha-gamma coincidence measurements was about 0.9 Bq for ^{239}Pu (51.6 keV) and 0.2 Bq for ^{240}Pu (45.2 keV), assuming P_α and P_β probabilities of 5%. However, for samples that do not contain ^{241}Am, the MDA would have been essentially lower, and an improvement of one order of magnitude is expected for ^{239}Pu. Detection of ^{239}Pu (51.6 keV) is sensitive to the amount of ^{241}Am in the sample because the peak is located in the energy domain that has considerable interference due to the scattering of 59.5 keV ^{241}Am gamma rays. For comparison, ^{240}Pu could not be detected at all by a singles gamma-ray data acquisition in a lead castle [88].

5.4 Conclusions

The sensitivity of non-destructive analysis of particulate samples can be significantly improved with alpha-gamma coincidence spectrometry. For low-active samples, the alpha-gated gamma-ray spectrum is almost free of external background even if the data acquisition lasts for weeks. Therefore, the small numbers of low-energy gamma rays are not masked by the statistical fluctuations of the background, allowing the detection of lower activities as compared with singles gamma-ray measurements.

Alpha-gamma coincidence spectrometry also tolerates the presence of fission products in the sample, i.e., they do not complicate the analysis of alpha-particle-emitting nuclides.

Compared to alpha-particle spectrometry, alpha-gated gamma-ray spectrometry depends significantly less on the sample geometry. Since the alpha particles are only used for triggering a gamma-ray measurement, the alpha-particle resolution has no impact on the analysis. For example, alpha-gamma coincidence spectrometry can be used to determine the ^{239}Pu and ^{240}Pu activities from micrometre-sized particles. For comparison, the analysis of the same sample with alpha-particle spectrometry requires destructive sample preparation due to the energy absorption of alpha particles in the sample. However, for perfectly thin samples, high-resolution alpha-particle spectrometry is typically more sensitive than alpha-gated gamma-ray spectrometry.

6. UV-gamma coincidence

UV-gamma coincidence is a novel approach invented in this thesis research to extend the use of alpha-gamma coincidence measurements. The main limitation of conventional alpha-gamma coincidence is the short range of alpha particles in air. However, alpha particles produce secondary UV radiation during their absorption in air. In the new method, these secondary UV photons are used to trigger the gamma-ray spectrometry measurement instead of the alpha particle itself. Thus, the range limitation of conventional alpha-gamma coincidence measurements can be overcome.

6.1 Alpha-induced UV fluorescence

The appearance of faint alpha-induced light in the vicinity of radioactive sources has been known for decades [89, 90, 91, 92]. When alpha particles travel in air, the Coulombic interaction with electrons leads to the ionization of atmospheric molecules. Furthermore, part of the initial alpha-particle energy is transferred to the kinetic energy of the ionization-induced free electrons, which in turn produce more ionization and lead to the excitation of atmospheric molecules. Some of these excited states

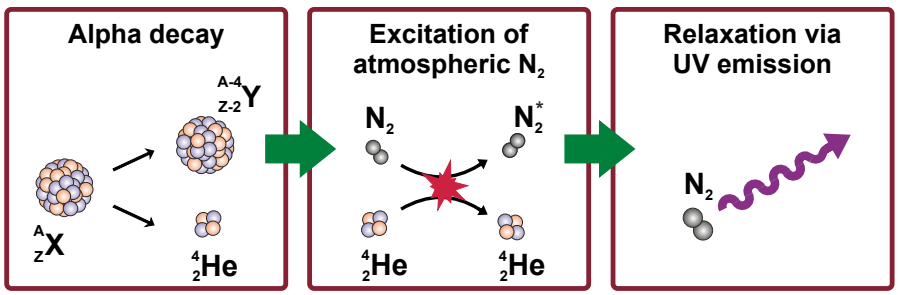

Figure 6.1. Principle of radioluminescence in air.

decay by radiating optical photons. The principle of the phenomenon is presented in Figure 6.1.

Most of the alpha-induced light is emitted in the near-UV region between 300–400 nm [93]. This is due to nitrogen molecules, the fluorescence properties of which are well known and have been investigated by several authors [94, 95]. Fluorescence emission wavelengths of diatomic nitrogen are determined by the electronic, vibrational and rotational states of the molecule. Under normal atmospheric conditions and after collisional excitation, the 2P and 1N band systems are usually observed. These consist of vibronic (electronic-vibrational) transitions of neutral and ionized nitrogen, respectively. The most intense emissions occur at wavelengths of 316, 337, 358 and 391 nm [95].

The fluorescence radiation from nitrogen is quenched by atmospheric oxygen and water vapour [94, 95]. Consequently, the summed energy emitted by the optical photons divided by the energy of the alpha particle is of the order of 10^{-5} in air [96]. According to the joint studies by STUK and the Optics Laboratory of Tampere University of Technology, one alpha particle with an energy of 5.5 MeV induces around 100 UV photons. These photons are born within a time interval of 5 ns [97]. In pure nitrogen or noble gas environment, the fluorescence yield is significantly higher [94, 98, 99].

Detection of secondary UV radiation has several advantages over direct alpha-particle measurement. Unlike alpha particles, induced UV photons travel long distances in air and can even penetrate transparent objects. The large number of UV photons produced per alpha decay also helps to achieve a good detection efficiency, which can be easily further increased by collecting the photons with lenses and mirrors. However, the UV photons do not carry nuclide-specific information. In addition, the measurements are easily disturbed by external lighting.

Review of applications During recent years, secondary UV radiation has been actively applied to the stand-off detection of alpha-particle-emitting radionuclides. Lamadie et al. [100] demonstrated that a CCD camera can be used to image the distribution of alpha contamination in field. The tests were carried out at nuclear facilities in operation or under decommissioning. Chister et al. [101] studied the capabilities of an Electron Multiplying CCD camera for the imaging of radioactive sources. The EM stage of the camera mitigates the CCD read noise and enables short exposure times, which are practical for field use. Closest to

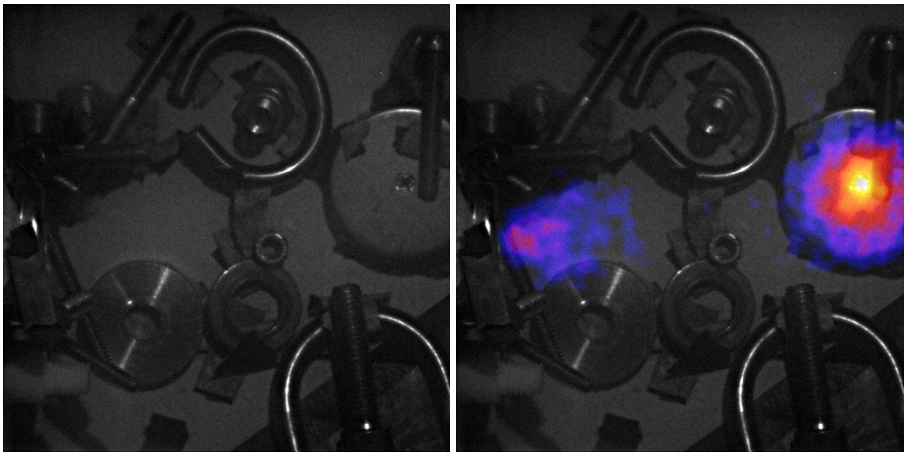

Figure 6.2. Scrap metal containing two ^{241}Am sources photographed with an Electron Multiplying CCD camera sensitive for alpha-induced UV photons. Left: A normal day-light image. Right: The same image combined with a false-colour UV image.

a commercial product, alpha-induced UV imaging has been developed by Bubble Technology Industries [102]. Their prototype, especially designed for near-field, wide-angle imaging, utilises a large aperture collection optics and pixelated (8x8) PMT mounted on a motorised panorama head. Long-range alpha-particle imaging was demonstrated outdoors by Layborne et al. [103]. They proved that 37 MBq ^{210}Po sources can be detected at a distance of 150 m by using photons having wavelengths short enough (<300 nm) not to be interfered with by sunlight.

Camera-based detection of alpha-particle emitters has also been studied in the joint research projects between STUK and the Optics Laboratory of Tampere University of Technology in 2008-2013. The capabilities of an Electron Multiplying CCD camera have been investigated in various measurement configurations in laboratory settings (see Figure 6.2). Furthermore, the camera has been applied to the detection of alpha-particle-emitting sources inside a glove box.

Besides imaging, several methods based on alpha-induced UV photons have been developed in these joint research projects. The capabilities of UV-gamma coincidence are discussed in Section 6.2. A portable device built for remote surface contamination screening is capable of distinguishing alpha-induced UV photons from artificial background lighting [98]. The device uses filtration to register photons in nitrogen fluorescence wavelengths and the background signal with separate photomultiplier tubes.

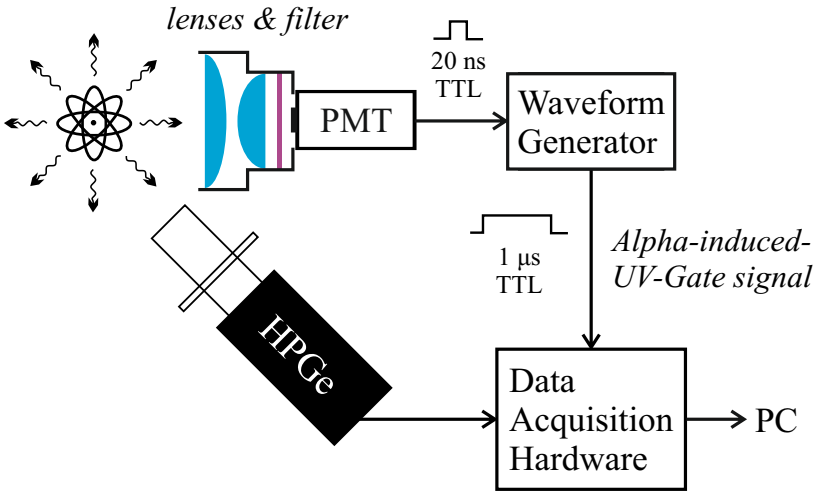

Figure 6.3. Principle of UV-gamma coincidence measurement for source characterisation. Adapted from Publication V.

6.2 Capabilities of UV-gamma coincidence

The capabilities of the UV-gamma coincidence approach were studied in two series of tests presented in Publications IV and V. The increase in sensitivity obtained by using UV photons was investigated by repeating the same gamma-ray measurements both with and without a UV coincidence trigger. Experiments with multiple sources were carried out to study the possibilities to focus a gamma-ray measurement on a single spot.

Figure 6.3 presents the principle of the measurement setup used. In all experiments, weak ^{241}Am sources were measured at distances longer than the alpha-particle range in air. The UV photons were measured with a photomultiplier tube and the gamma-rays with a HPGe detector. The coincidence resolving times used varied from 1 to 8 µs. To achieve reasonably efficiency, UV photons were collected in the photomultiplier with lenses. The gamma-ray background was increased with disturbing sources to simulate the conditions typical of safeguards measurements. Even though the technique was demonstrated with ^{241}Am, the results are equally valid for other sources producing gamma rays in coincidence with alpha particles.

Detection of low-activity sources The UV-gated gamma-ray measurement was demonstrated to be more sensitive to the ^{241}Am sources with low activity than the singles gamma-ray measurement. The intensity of the 59.5 keV gamma-ray peak of ^{241}Am was negligible without the UV

Table 6.1. Comparison of singles and UV-gated gamma-ray measurements. Adapted from Publication V.

	Singles	Gated
Peak area (counts)	35100 ± 1600	1375 ± 74
Background area (counts)	639600 ± 1600	43 ± 13
Currie's L_c (counts)	1316	11
Signal-to-noise ratio	0.047	27.5
Peak significance	22.9	109
MDA (Bq)	3.8	0.88

gate (see Figure 6.4a) but clearly visible in the UV-gated spectrum (see Figure 6.4b). Analyses of the spectra (see Table 6.1) revealed the reason for the increase in sensitivity: although the UV gate greatly reduced the photo-peak signal, the reduction in the background was over 500 times more intense. For example, an acquisition time of 40 h would have been required to reach an MDA of 3.8 Bq without the UV gate, whereas with the UV gate, the same MDA could have been reached in less than 4 h. The random coincidences dominating the gated background were caused by thermal noise or illumination that frequently triggered the UV detector.

The X-ray part of the spectrum is important for the detection of plutonium, even though it only contains elemental information. The L X-ray intensities per alpha decay are comparable for ^{239}Pu, ^{240}Pu and ^{241}Am, but the gamma-ray yields for Pu are several orders of magnitude lower than for ^{241}Am. The detection of plutonium X-rays would only have been possible in a low-background spectrum achieved with the UV gate (Figure 6.4b). The L X-rays of both plutonium and americium have energies in the range of 12-20 keV, but these can still be distinguished from each other with advanced spectrum deconvolution [104].

According to the tests conducted, UV-gated gamma-ray measurements can be performed either in darkness or in dim LED lighting. In LED lighting, wavelength-specific filtration of the light collected in the photomultiplier was required. The filter applied transmitted the most intense emissions of the nitrogen fluorescence at near-UV wavelengths (316, 337 and 358 nm) but blocked visible light. The LED light source was selected to emit a minimal quantity of disturbing photons in the near-UV region. The coincidence measurement was not as sensitive to the background light as similar singles UV measurements because the

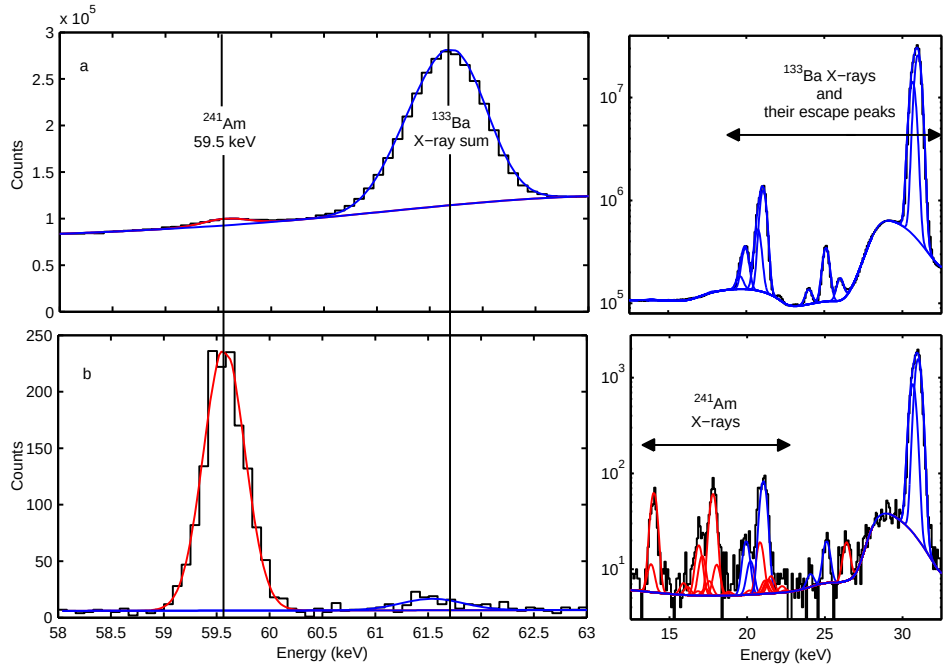

Figure 6.4. Singles (a) and UV-gated (b) gamma-ray spectrum of the 59.5 keV ^{241}Am line. The X-ray parts of the same spectra are also shown. The measurements were performed in a high gamma-ray background generated with ^{133}Ba. The ^{133}Ba peaks in the gated spectrum are caused by random coincidences. Adapted from Publication V.

short coincidence resolving time efficiently reduced the rate of random coincidences.

The UV-gated gamma-ray measurement was successfully repeated for a sample inside a transparent plastic bag. Since 75% of the UV photons penetrated the packing, the signal was not significantly attenuated as long as the air volume inside the packing was sufficient to absorb the alpha particles. About five times higher count rates were obtained by replacing the air around the source with pure nitrogen.

Focused gamma-ray measurement The UV gate was also shown to efficiently focus the gamma-ray measurement on a single spot. Adding two extra ^{241}Am sources next to the source of interest increased the count rate by only 20%, even though the activity of the extra sources was about 10 times higher compared to the activity of the original ^{241}Am source. The phenomenon was investigated in detail by moving an ^{241}Am source perpendicular to the focal axis of the UV detector. The UV efficiency fell below one tenth when the source was only 50 mm off-focus of the UV detector.

6.3 Conclusions

UV-gamma coincidence measurement shares the same advantages as conventional alpha-gamma coincidence measurement. Triggering a gamma-ray measurement with alpha-particle-induced UV photons focuses the gamma-ray measurement to a single spot and suppresses the signal from isotopes not decaying by alpha-particle emission. Due to the remarkable reduction of disturbing background, smaller activities of alpha-particle-emitting radionuclides can be detected.

The most significant advantage of the technique based on the use of secondary optical UV photons over alpha particles is the long range of optical photons in air. Thus, the measurement geometry is not limited by the alpha-particle range. When absorbed in air, one alpha particle produces about 100 UV photons, which helps to obtain a reasonable efficiency. In principle, the only crucial criteria for a successful measurement are the release of alpha particles to air and the line-of-sight between the UV detector and the source. In practice, the low efficiency at long distances limits the feasible measurement range, even though the collection of optical photons can be enhanced with lenses and mirrors. A further restriction is the requirement of low optical background on nitrogen fluorescence wavelengths. This limits the usability of the method to dark or artificially illuminated environments.

7. Discussion and conclusions

The studies presented in this thesis showed that radiometric approaches have unused potential for the analysis of nuclear and other radioactive materials. The reliability of the analyses is improved by taking the correlations between variables into account both in spectrum fitting and in the interpretation of the results. With coincidence techniques, superior measurement sensitivity is obtained from the same detectors commonly used for data acquisition.

For uncertainty estimation in spectrum analysis, the most accurate method was shown to be the covariance calculus of all unknown parameters. This method produces unbiased and statistically correct estimates for peak areas and their uncertainty estimates. This also applies for peak multiplets, a case where commercial spectrum analysis software typically fails [38, 49]. The approach was implemented in two spectrum analysis software programs that also utilise nuclide data maximally to reduce the number of fitted parameters: AMUFI for gamma-rays spectra and ADAM for alpha-particle spectra.

In previous studies, determining the ^{239}Pu/^{240}Pu isotopic ratio from samples with an activity of only a few becquerels has been regarded as extremely challenging with radiometric methods. Distinguishing between these two isotopes is generally considered impossible with alpha-particle spectrometry, since their main alpha-particle peaks differ only by 12 keV in energy, which is of the same order of magnitude or less than the resolution of typical semiconductor detectors. Gamma-ray spectrometry is also inefficient for plutonium analysis, since the gamma-ray emissions of low energy and yield are masked by the background.

In this thesis, high-resolution alpha-particle spectrometry together with the spectrum analysis with ADAM was shown to be able to determine the ^{239}Pu/^{240}Pu isotopic ratio. For reliable results, the number of counts in

the ^{239,240}Pu peak group must be larger than 1000. It should be kept in mind that this approach is only valid for superior thin samples. For lower-quality samples, the energy absorption of alpha particles in the sample matrix makes it impossible to distinguish between alpha-particle emission energies close to each other.

For low-quality samples that cannot be characterised with gamma-ray or alpha-particle spectrometry alone, the alpha-gamma coincidence approach was shown to be efficient. A gamma-ray spectrum gated with alpha particles is almost free from external background, allowing the detection of very small signals. The technique was demonstrated to be suitable for determining the relative and absolute concentrations of different plutonium isotopes from a micrometre-sized particle with a total plutonium activity of only 4 Bq. Moreover, the coincidence technique reduces the uncertainties related to the measurement geometry, increasing the accuracy of the activity results.

The strict geometry requirements for alpha-particle measurements can be further reduced by using secondary UV photons instead of alpha particles themselves to trigger a gamma-ray measurement. The secondary UV photons are produced during the alpha-particle absorption in air. The method allows analyses of isotopes decaying by alpha-particle emission from distances greater than the range of alpha particles in air. Together with a UV-transmitting filter, a photomultiplier tube can be operated for alpha-particle detection under LED lighting. Because UV radiation penetrates several transparent materials, the method is also suited for the analysis of samples inside closed packing.

7.1 Implications

The new techniques for spectrum deconvolution can significantly extend the in-field analysis capabilities. In field conditions, the best detectors and complex sample manipulation procedures are not feasible. Therefore, reliable area and uncertainty estimations for overlapping peaks become crucial. The capability of handling overlapping peaks increases the usability of medium-resolution gamma-ray detectors for the analyses of sources consisting of multiple radioactive isotopes. In alpha-particle spectrometry, a reliable spectrum deconvolution method cuts down the requirements for sample quality and opens up the possibilities for rapid characterisation of the alpha-particle emitting isotopes. When broader,

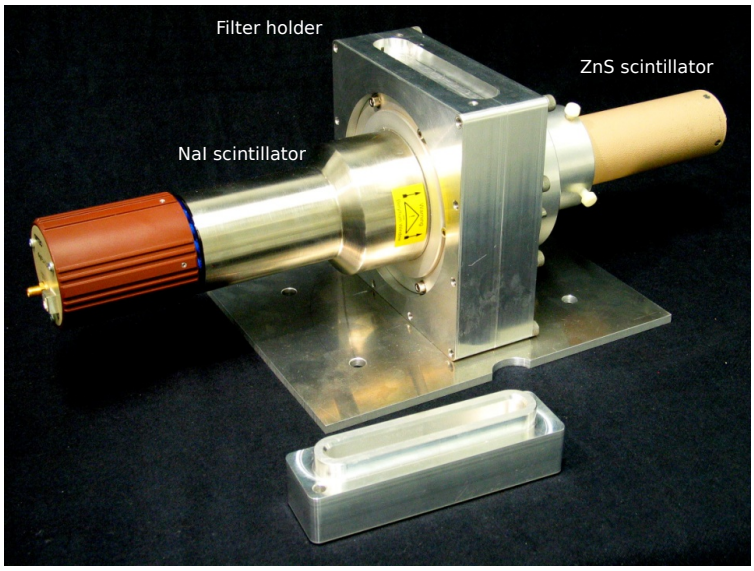

Figure 7.1. Simple alpha-gamma coincidence measurement device for the detection of low ^{241}Am concentrations in air.

overlapping peaks can be tolerated, the chemical separation of the elements in the sample is not necessarily required. Even non-destructive alpha-particle analysis without any sample manipulation is sometimes feasible, but this also requires the utilisation of sampling methods that minimise the alpha-particle absorption in the sample matrix [105].

The alpha-gamma coincidence approach is especially suited for the detection of transuranium elements in particulate samples. Therefore, the IAEA safeguards analytical laboratory has also shown interest in this technique [81]. Coincidence measurement with high-resolution detectors in a vacuum could be an efficient method for the screening of safeguards samples. In addition to the traditional high-resolution alpha-particle and gamma-ray spectra, a single measurement would simultaneously produce the data for coincidence analysis. Due to the larger L X-ray yields of plutonium isotopes compared to the gamma-ray yields, the X-ray region between 11-21 keV is the most sensitive indicator for plutonium in gated measurements. The X-rays do not contain isotope-specific information, but knowing the elements present is already valuable for screening purposes.

At STUK, the alpha-gamma coincidence technique has been further adapted for the detection of ^{241}Am in air for occupational safety purposes (see Figure 7.1). During 2012, a simple prototype was successfully operated at a steel melting shop. In this prototype, the air filter samples are measured in a close geometry between a ZnS scintillator alpha-particle detector and a NaI scintillator gamma-ray detector.

An obvious usage for secondary UV radiation is the screening of contaminated surfaces. Screening of large areas is a laborious task with a conventional alpha-particle detector, since the detector must be brought to within a few centimetres of the source to obtain any signal. Compared to the strict geometry requirements in direct alpha-particle measurement, the UV technique offers significant flexibility. In particular, the decommissioning of nuclear facilities and crime-scene investigation would greatly benefit from the detection and analysis of alpha contamination at a stand-off distance.

The UV-gamma method is feasible for sample analysis in measurement geometries not allowing the use of traditional alpha-particle detectors. For example, the technique can be used for the detection and identification of fissile materials inside a glove box with detectors outside the box. The feasibility of UV imaging has already been demonstrated in this environment [100]. A further potential application is the analysis of swipe samples without opening the sealed plastic bags or other transparent packings. This is especially important in nuclear safeguards and forensics, since it guarantees the integrity of the samples and prevents cross-contamination [14, 8].

7.2 Limits of the techniques

In coincidence techniques, the increase in sensitivity is always obtained via background reduction. However, the background is reduced at the cost of efficiency. Therefore, the techniques are better suited for long measurements in a high gamma-ray background than for short measurements in a low background. Additionally, the high efficiency of both detectors is emphasised. To minimise the background produced by random coincidences, it is favourable to use fast detectors allowing shorter coincidence time windows.

Even though the secondary UV photons remove the range restriction of alpha-particle detection, the efficiency still limits the usable range of UV-gamma coincidence measurements. As with all coincidence methods, the UV-gamma coincidence approach improves MDA most when the source-to-detector distance is short. Far from the source, the detection efficiency in a singles gamma-ray measurement is inversely proportional to the distance squared. In a gated measurement, the efficiency is inversely proportional to the distance to the power of four. The loss in efficiency can

be somewhat compensated in stand-off UV measurements by improving the UV collection with larger lenses. As a rule of thumb, improving MDA with the coincidence method becomes challenging if the source-to-detector distance exceeds one metre.

The UV-gated gamma-ray measurement also has some further limitations. First, the background caused by lighting restricts the use of the technique. Currently, the method can only be applied in a dark or artificially illuminated environment. The wavelength of the artificial illumination must be designed not to disturb the UV signal caused by radioactive sources. Second, the absorption of the alpha particles must take place in air. Even covering the source with paint may be enough to absorb the alpha particles and prevent the formation of UV photons. However, the capability to measure only the activity directly on the surface is a great advantage in certain applications. This distinction is especially important for radiation safety, since surface contamination poses a higher health risk than sealed sources.

7.3 Future research

In the future, it is expected that other analysis programs will take the uncertainty estimation method presented in this thesis into use. Recently, two gamma-ray spectrum analysis programs have already started to deploy the same approach [106, 107]. In addition to gamma-ray and alpha-particle spectrometry, software packages for resolving conversion electron spectra are required. Conversion electron spectrometry has been shown to have great potential for plutonium analysis [108, 109], but proper tools for spectrum deconvolution are not available.

Research on various coincidence measurement approaches has recently been active. However, much less effort has been placed on coincidence data analysis. In the future, significant investment in the development of coincidence analysis is required to maximally utilise the collected data. For example, the coincidence data analysis is still based on ordinary spectra created with various gating criteria. Instead of analysing ordinary spectra, the whole event data set should be compared against the expected nuclide response. Another significant shortage in the analysis is the use of Gaussian statistics, which is not valid for data consisting of a few counts. The problem is significant in coincidence analysis, since the negligible background allows the detection of very small signals.

In alpha-particle measurements employing secondary UV radiation, the main challenge is to find efficient ways to reduce the background caused by lighting. Currently, the most promising approach is to select the recorded UV wavelengths carefully. Since wavelengths below 280 nm are not disturbed by sunlight, it would be a breakthrough to find notable alpha-induced emissions at these solar-blind wavelengths. Therefore, optical emissions in different gas mixtures should be studied. In coincidence techniques, the background can also be reduced by using very fast detectors and acquisition electronics, allowing the use of shorter coincidence time windows.

Bibliography

[1] J. van der Veen et al. “Core fragments in Chernobyl fallout”. In: *Nature* 323.6087 (1986), pp. 399–400.

[2] M. Levi and H. Kelly. “Weapons of mass disruption”. In: *Scientific American* 287.5 (2002), pp. 76–81.

[3] R. Stone. “State-of-the-Art Nuclear Sleuths”. In: *Science* 300.5626 (2003), pp. 1643–1643.

[4] *Terminology Used in Nuclear Safety and Radiation Protection*. International Atomic Energy Agency (IAEA), 2007.

[5] *Nuclear Security Fundamentals, Objective and Essential Elements of a State’s Nuclear Security Regime*. International Atomic Energy Agency (IAEA), 2013.

[6] *IAEA Safegurds Glossary, 2001 Edition*. International Atomic Energy Agency (IAEA), 2002.

[7] H. Maguire et al. “Assessing public health risk in the London polonium-210 incident, 2006”. In: *Public Health* 124.6 (2010), pp. 313–318.

[8] *Nuclear Forensics Support, Reference Manual*. International Atomic Energy Agency (IAEA), 2006.

[9] F. Padoani et al. “Setting up and implementation of a global atmospheric radioactivity monitoring network for CTBT verification purposes”. In: *Journal of Radioanalytical and Nuclear Chemistry* 263.1 (2005), pp. 183–188.

[10] M. Auer et al. “Ten years of development of equipment for measurement of atmospheric radioactive xenon for the verification of the CTBT”. In: *Pure and Applied Geophysics* 167.4-5 (2010), pp. 471–486.

[11] P. Richards and W.-Y. Kim. “Seismic signature”. In: *Nature Physics* 3.1 (2007), pp. 4–6.

[12] N. Brachet et al. “Monitoring the earth’s atmosphere with the global IMS infrasound network”. In: Infrasound Monitoring for Atmospheric Studies. 2009, pp. 77–118.

[13] M. W. Lawrence and P. Grenard. “Hydroacoustic monitoring system for the Comprehensive Nuclear-Test-Ban Treaty”. In: *OCEANS ’98 Conference Proceedings*. Vol. 2. 1998, 694–697 vol.2.

[14] *Safeguards Techniques and Equipment*. International Atomic Energy Agency (IAEA), 2011.

[15] M. Rees, B. Koppelman, and N. Davison. “Scientific steps to nuclear disarmament”. In: *Nature* 465.7296 (2010), pp. 290–291.

[16] *Nuclear Security Systems and Measures for Major Public Events, Implementing Guide*. International Atomic Energy Agency (IAEA), 2012.

[17] K. Mayer, M. Wallenius, and I. Ray. “Nuclear forensics-a methodology providing clues on the origin of illicitly trafficked nuclear materials”. In: *Analyst* 130.4 (2005), pp. 433–441.

[18] F. Stanley, A. Stalcup, and H. Spitz. “A brief introduction to analytical methods in nuclear forensics”. In: *Journal of Radioanalytical and Nuclear Chemistry* 295.2 (2013), pp. 1385–1393.

[19] *Stopping Power and Ranges for Protons and Alpha Particles (Report 49)*. International Commission on Radioation Units (ICRU), 1993.

[20] L. Currie. “Limits for qualitative detection and quantitative determination. Application to radiochemistry”. In: *Analytical Chemistry* 40.3 (1968), pp. 586–593.

[21] L. Currie. “On the detection of rare, and moderately rare, nuclear events”. In: *Journal of Radioanalytical and Nuclear Chemistry* 276.2 (2008), pp. 285–297.

[22] G. John. *Multi-Agency Radiological Laboratory Analytical Protocols Manual (NUREG-1576), Technical Report*. 2004.

[23] S. Chatterjee and J. Simonoff. *Handbook of Regression Analysis*. Vol. 5. John Wiley & Sons, 2013.

[24] *OIML 2008 Evaluation of Measurement Data—Guide to the Expression of Uncertainty in Measurement*. Joint Committee for Guides in Metrology (JCGM), 1995.

[25] S. L. Ellison and A. Williams. *Eurachem/CITAC guide: Quantifying Uncertainty in Analytical Measurement, Third edition*. Eurachem, 2012.

[26] D. V. Hinkley. "On the ratio of two correlated normal random variables". In: *Biometrika* 56.3 (1969), pp. 635–639.

[27] E. Fieller. "The biological standardization of insulin". In: *Supplement to the Journal of the Royal Statistical Society* 7.1 (1940), pp. 1–64.

[28] S. Ali et al. "Ultrahigh energy resolution gamma-ray spectrometers for precision measurements of uranium enrichment". In: *Journal of Radioanalytical and Nuclear Chemistry* 276.3 (2008), pp. 749–753.

[29] E. Van Loef et al. "Scintillation properties of LaBr3:Ce3+ crystals: Fast, efficient and high-energy-resolution scintillators". In: *Nuclear Instruments and Methods in Physics Research, Section A: Accelerators, Spectrometers, Detectors and Associated Equipment* 486.1-2 (2002), pp. 254–258.

[30] N. Cherepy et al. "Scintillators with potential to supersede lanthanum bromide". In: *Nuclear Science, IEEE Transactions on* 56.3 (2009), pp. 873–880.

[31] T. Schlesinger et al. "Cadmium zinc telluride and its use as a nuclear radiation detector material". In: *Materials Science and Engineering: R: Reports* 32.4–5 (2001), pp. 103–189.

[32] H. Chen et al. "Characterization of large cadmium zinc telluride crystals grown by traveling heater method". In: *Journal of Applied Physics* 103.1 (2008), pp. 014903–014903–5.

[33] P. Aarnio, M. Nikkinen, and J. Routti. "UNISAMPO, comprehensive software for gamma-spectrum processing". In: *Journal of Radioanalytical and Nuclear Chemistry* 248.2 (2001), pp. 371–375.

[34] D. Arnold et al. "The 2002 IAEA intercomparison of software for low-level gamma-ray spectrometry". In: *Nuclear Instruments and Methods in Physics Research Section A: Accelerators, Spectrome-*

ters, Detectors and Associated Equipment 536.1–2 (2005), pp. 196–210.

[35] Ortec. *GammaVision v6.09 brochure*. 2013.

[36] *Radionuclide analysis and evaluation software Aatami, software version 4.10, Users Manual*. 2007.

[37] J. Routti and S. Prussin. “Photopeak method for the computer analysis of gamma-ray spectra from semiconductor detectors”. In: *Nuclear Instruments and Methods in Physics Research Section A: Accelerators, Spectrometers, Detectors and Associated Equipment* 72.2 (1969), pp. 125–142.

[38] *Intercomparison of Gamma Ray Analysis Software Packages, IAEA TECDOC 1010*. International Atomic Energy Agency (IAEA), 1998.

[39] CTBTO. *Reference Manual of Radionuclide Analysis and Evaluation Software Aatami, v 4.10*. Tech. rep. 2007.

[40] P. Aarnio et al. “Linssi: Database for gamma-ray spectrometry”. In: *Journal of Radioanalytical and Nuclear Chemistry* 276.3 (2008), pp. 631–637.

[41] T. Burr et al. “Smoothing low resolution gamma spectra”. In: *Nuclear Science, IEEE Transactions on* 57.5 (2010), pp. 2831–2840.

[42] L.-E. De Geer. “Currie detection limits in gamma-ray spectroscopy”. In: *Applied Radiation and Isotopes* 61.2–3 (2004), pp. 151–160.

[43] L.-E. De Geer. “Radionuclide evidence for low-yield nuclear testing in North Korea in April/May 2010”. In: *Science and Global Security* 20.1 (2012), pp. 1–29.

[44] G. Wotawa. “Meteorological analysis of the detection of xenon and barium/lanthanum isotopes in May 2010 in Eastern Asia”. In: *Journal of Radioanalytical and Nuclear Chemistry* 296 (2013), pp. 339–347.

[45] C. M. Wright. “Low-yield nuclear testing by North Korea in May 2010: Assessing the evidence with atmospheric transport models and xenon activity calculations”. In: *Science and Global Security* 21.1 (2013), pp. 3–52.

[46] D. Schaff, W.-Y. Kim, and P. Richards. “Seismological constraints on proposed low-yield nuclear testing in particular regions and time periods in the past, with comments on "Radionuclide evidence for low-yield nuclear testing in North Korea in April/May 2010" by Lars-Erik De Geer”. In: *Science and Global Security* 20.2-3 (2012), pp. 155–171.

[47] M. L’Annunziata. *Handbook of Radioactivity Analysis, Second Edition*. Academic Press, 2003.

[48] E. García-Toraño. “Current status of alpha-particle spectrometry”. In: *Applied Radiation and Isotopes* 64.10–11 (2006), pp. 1273–1280.

[49] *Intercomparison of Alpha Particle Spectrometry Software Packages. IAEA TECDOC Series no 1104*. International Atomic Energy Agency (IAEA), 1999.

[50] R. C. Noy et al. “The WinALPHA code for the analysis of alpha-particle spectra”. In: *Nuclear Instruments and Methods in Physics Research Section A: Accelerators, Spectrometers, Detectors and Associated Equipment* 525.3 (2004), pp. 522–528.

[51] N. Vajda and C.-K. Kim. “Determination of Pu isotopes by alpha spectrometry: a review of analytical methodology”. In: *Journal of Radioanalytical and Nuclear Chemistry* 283.1 (2010), pp. 203–223.

[52] S. Srinivasan et al. “Determination of the Pu-240/Pu-239 ratio by alpha spectrometry using the WinALPHA program”. In: *Applied Radiation and Isotopes* 64.5 (2006), pp. 591–593.

[53] S. LaMont, S. Glover, and R. Filby. “Determination of plutonium-240/239 ratios in low activity samples using high resolution alpha-spectrometry”. In: *Journal of Radioanalytical and Nuclear Chemistry* 234.1 (1998), pp. 195–199.

[54] P. Mitchell et al. “Determination of the Cm-243/Cm-244 ratio alpha spectrometry and spectral deconvolution in environmental samples exposed to discharges from the nuclear fuel cycle”. In: *Applied Radiation and Isotopes* 49.9 (1998), pp. 1283–1288.

[55] G. Bortels et al. *EUROMET Project No 325: Analysis of Plutonium Alpha-Particle Spectra (Internal Report)*. IRMM, 1996.

[56] G. Bortels, C. Hurtgen, and D. Santry. “Nuclide analysis on low-statistics alpha-particle spectra: an experimental verification for Pu isotopes”. In: *Applied Radiation and Isotopes* 46.11 (1995), pp. 1135–1144.

[57] W. Raab and J. Parus. “The measurement of Pu-240/Pu-239 and Pu-238/Pu-239 isotopic ratios by alpha-particle spectrometry”. In: *Nuclear Instruments and Methods in Physics Research Section A: Accelerators, Spectrometers, Detectors and Associated Equipment* 339.1 (1994), pp. 116–121.

[58] S. Aggarwal and D. Alamelu. “High resolution alpha-particle spectrometry for the determination of Pu-240/Pu-239 atom ratio in Pu samples from PHWR”. In: *Journal of Alloys and Compounds* 444 (2007), pp. 656–659.

[59] Z. Lin et al. “Competence of alpha spectrometry analysis algorithms used to resolve the Am-241 and Am-243 alpha peak overlap”. In: *Applied Radiation and Isotopes* 56.1 (2002), pp. 57–63.

[60] G. Bortels and P. Collaers. “Analytical function for fitting peaks in alpha-particle spectra from Si detectors”. In: *Applied Radiation and Isotopes* 38.10 (1987), pp. 831–837.

[61] A. Martín Sánchez, F. Vera Tomé, and P. Rubio Montero. “Fitting of alpha spectra. Application to low-level measurements”. In: *Applied Radiation and Isotopes* 47.9 (1996), pp. 899–903.

[62] F. Dayras. “Analysis of Pu-239, Cm-244 and Am-243 alpha spectra using the unfolding code Colégram without prior use of a nuclear data library”. In: *Nuclear Instruments and Methods in Physics Research Section A: Accelerators, Spectrometers, Detectors and Associated Equipment* 490.3 (2002), pp. 492–504.

[63] T. Siiskonen and R. Pöllänen. “Alpha–electron and alpha–photon coincidences in high-resolution alpha spectrometry”. In: *Nuclear Instruments and Methods in Physics Research Section A: Accelerators, Spectrometers, Detectors and Associated Equipment* 558.2 (2006), pp. 437–440.

[64] *AASI, Advanced Alphaspectrometric Simulation, sortware version 1.1, User’s manual*. 2008.

[65] R. Pöllänen et al. “Activity determination without tracers in high-resolution alpha-particle spectrometry”. In: *Journal of Radioanalytical and Nuclear Chemistry* (2011).

[66] A. Martín Sánchez and P. Rubio Montero. “Simplifying data fitting using branching ratios as constraints in alpha spectrometry”. In: *Nuclear Instruments and Methods in Physics Research Section A: Accelerators, Spectrometers, Detectors and Associated Equipment* 420.3 (1999), pp. 481–488.

[67] E. García-Toraño. “Fitting of low-statistics peaks in alpha-particle spectra”. In: *Nuclear Instruments and Methods in Physics Research Section A: Accelerators, Spectrometers, Detectors and Associated Equipment* 339.1 (1994), pp. 122–126.

[68] W. Zhang et al. “Performance evaluation and optimization for a newly developed digital list-mode data acquisition Compton suppression spectrometer”. In: *Applied Radiation and Isotopes* 81 (2013), pp. 96–102.

[69] K. J. Thomas et al. “Installation of a muon veto for low background gamma spectroscopy at the LBNL low-background facility”. In: *Nuclear Instruments and Methods in Physics Research Section A: Accelerators, Spectrometers, Detectors and Associated Equipment* 724.0 (2013), pp. 47–53.

[70] J. Burnett and A. Davies. “Compton suppressed gamma-spectrometry for Comprehensive Nuclear-Test-Ban Treaty samples”. In: *Journal of Radioanalytical and Nuclear Chemistry* 295.1 (2013), pp. 497–499.

[71] J. Burnett, A. Davies, and J. McLarty. “Further development of a cosmic veto gamma-spectrometer”. In: *Journal of Radioanalytical and Nuclear Chemistry* (2013), pp. 1–6.

[72] G. Lutter et al. “A new versatile underground gamma-ray spectrometry system”. In: *Applied Radiation and Isotopes* (2013).

[73] R. Britton. “Compton suppression systems for environmental radiological analysis”. In: *Journal of Radioanalytical and Nuclear Chemistry* 292.1 (2012), pp. 33–39.

[74] A. Bernstein et al. “Monitoring the thermal power of nuclear reactors with a prototype cubic meter antineutrino detector”. In: *Journal of Applied Physics* 103.7 (2008), p. 074905.

[75] A. Ringbom et al. “SAUNA—a system for automatic sampling, processing, and analysis of radioactive xenon”. In: *Nuclear Instruments and Methods in Physics Research Section A: Accelerators, Spectrometers, Detectors and Associated Equipment* 508.3 (2003), pp. 542–553.

[76] G. Petit et al. “Innovative concept for a major breakthrough in atmospheric radioactive xenon detection for nuclear explosion monitoring”. In: *Journal of Radioanalytical and Nuclear Chemistry* (2013), pp. 1–11.

[77] W. Zhang et al. “Quantification of U-235 and U-238 activity concentrations for undeclared nuclear materials by a digital gamma–gamma coincidence spectroscopy”. In: *Applied Radiation and Isotopes* 69.6 (2011), pp. 904–907.

[78] J. Konki et al. “Comparison of gamma-ray coincidence and low-background gamma-ray singles spectrometry”. In: *Applied Radiation and Isotopes* 70.2 (2012), pp. 392–396.

[79] W. Zhang et al. “A system for low-level the cosmogenic Na-22 radionuclide measurement by gamma–gamma coincidence method using BGO detectors”. In: *Journal of Radioanalytical and Nuclear Chemistry* 287.2 (2011), pp. 551–555.

[80] F. Heßberger et al. “Alpha-gamma decay studies of No-255”. In: *The European Physical Journal A-Hadrons and Nuclei* 29.2 (2006), pp. 165–173.

[81] K. Breitenecker et al. “Configuration of an alpha–gamma coincidence spectrometer for utilization of safeguards measurements”. In: *Applied Radiation and Isotopes* 67.12 (2009), pp. 2088–2091.

[82] G. F. Knoll. *Radiation detection and measurement, Third Edition*. John Wiley & Sons, 2000.

[83] J. Turunen et al. “PANDA—A novel instrument for non-destructive sample analysis”. In: *Nuclear Instruments and Methods in Physics Research Section A: Accelerators, Spectrometers, Detectors and Associated Equipment* 613.1 (2010), pp. 177–183.

[84] J. Turunen et al. “Comprehensive radioassays of samples using the PANDA device”. In: *Nuclear Instruments and Methods in Physics Research Section A: Accelerators, Spectrometers, Detectors and Associated Equipment* 678 (2012), pp. 78–82.

[85] S. Ihantola et al. “Sample screening to locate active particles with position-sensitive alpha detector”. In: *Proceedings of the Third European IRPA Congress*. 2010, pp. 1967–1973.

[86] M. Eriksson. *On weapons plutonium in the Arctic environment (Thule, Greenland)*. Risø National Laboratory Roskilde, Denmark, 2002.

[87] O. Lind et al. “Characterization of uranium and plutonium containing particles originating from the nuclear weapons accident in Thule, Greenland, 1968”. In: *Journal of Environmental Radioactivity* 81.1 (2005), pp. 21–32.

[88] R. Pöllänen et al. “Direct alpha spectrometry for characterising hot particle properties”. In: *Radiation Measurements* 42.10 (2007), pp. 1666–1673.

[89] W. Huggins and L. Huggins. “On the spectrum of the spontaneous luminous radiation of radium at ordinary temperatures”. In: *Proceedings of the Royal Society of London* 72.477-486 (1903), pp. 196–199.

[90] R. Nicholls and E. Reeves. “Luminescence produced in air by polonium-210 alpha particles”. In: *Nature* 180.4596 (1957), pp. 1188–1189.

[91] G. Davidson and R. O’neil. “Optical radiation from nitrogen and air at high pressure excited by energetic electrons”. In: *The Journal of Chemical Physics* 41 (1964), p. 3946.

[92] I. Tatischeff. “Specific excitation of N2 and specific ionization by 4.3 MeV alpha particles”. In: *The Journal of Chemical Physics* 52 (1970), p. 503.

[93] S. M. Baschenko. “Remote optical detection of alpha particle sources”. In: *Journal of Radiological Protection* 24.1 (2004), p. 75.

[94] A. N. Bunner. *Cosmic ray detection by atmospheric fluorescence*. PhD Thesis. Cornell University, 1967.

[95] T. Waldenmaier. *Spectral resolved measurement of the nitrogen fluorescence yield in air induced by electrons*. 2006.

[96] P. P. Bachelor et al. “Self-absorption effects on alpha-induced atmospheric nitrogen fluorescence yield”. In: *Journal of Radioanalytical and Nuclear Chemistry* 282.3 (2009), pp. 873–876.

[97] J. Sand. *Properties and applications of alpha-radiation-induced fluorescence of air*. Master's Thesis. Tampere University of Technology, 2012.

[98] V. Hannuksela et al. "Optical remote detection of alpha radiation". In: *Proceedings of the Third European IRPA Congress*. 2010, pp. 1750–1756.

[99] O. Hoff. *Determination of alpha radiation-induced fluorescence efficiency*. Bachelor's Thesis. The University of Southern Mississippi, 2012.

[100] F. Lamadie et al. "Remote alpha imaging in nuclear installations: new results and prospects". In: *IEEE Transactions on Nuclear Science* 52.6 (2005), pp. 3035–3039.

[101] D. L. Chichester and S. M. Watson. "Multispectral UV-visual imaging as a tool for locating and assessing ionizing radiation in air". In: *Nuclear Science, IEEE Transactions on* 58.5 (2011), pp. 2512–2518.

[102] E. Inrig et al. "An air fluorescence imaging system for the detection of radiological contamination". In: *Proc. SPIE 8018, Chemical, Biological, Radiological, Nuclear, and Explosives (CBRNE) Sensing XII, 80180G*. Vol. 80180G. 2011.

[103] A. E. Leybourne et al. "Long range detection of radiation-induced air fluorescence". In: *Proceedings of the Institute of Nuclear Materials Management Annual Meeting*. 2010.

[104] S. Ihantola et al. "Screening samples with a position-sensitive detection system providing isotope-specific information". In: *Proceedings of the Symposium on International Safeguards, Preparing for Future Verification Challenges*. 2010.

[105] S. Ihantola. *Surface sampling methods for non-destructive radionuclide analysis*. Master's Thesis. Helsinki University of Technology, 2009.

[106] Canberra. *ProSpect gamma spectroscopy software data sheet*. 2013.

[107] R. Coldwell and G. Lasche. "Experimental comparisons of statistical uncertainties in analysis of nuclear spectra with the Cambio software application". In: *Journal of Radioanalytical and Nuclear Chemistry* 296.2 (2013), pp. 655–662.

[108] T. De Vol, A. Ringberg, and R. Dewberry. “Isotopic analysis of plutonium using a combination of alpha and internal conversion electron spectroscopy”. In: *Journal of Radioanalytical and Nuclear Chemistry* 254.1 (2002), pp. 71–79.

[109] K. Peräjärvi et al. “Feasibility of conversion electron spectrometry using a Peltier-cooled silicon drift detector”. In: *Journal of Radioanalytical and Nuclear Chemistry* In Press (2013).

Aalto-DD 198/2013

ISBN 978-952-60-5460-5
ISBN 978-952-60-5461-2 (pdf)
ISSN-L 1799-4934
ISSN 1799-4934
ISSN 1799-4942 (pdf)

Aalto University
School of Science
Department of Applied Physics
www.aalto.fi

BUSINESS +
ECONOMY

ART +
DESIGN +
ARCHITECTURE

SCIENCE +
TECHNOLOGY

CROSSOVER

**DOCTORAL
DISSERTATIONS**